

Chiral properties of (2+1)-flavor QCD in strong magnetic fields at zero temperature

H.-T. Ding^a, S.-T. Li^{b,a}, A. Tomiya^c, X.-D. Wang^a, Y. Zhang^a

^a*Key Laboratory of Quark and Lepton Physics (MOE) and Institute of Particle Physics, Central China Normal University, Wuhan 430079, China*

^b*Institute of Modern Physics, Chinese Academy of Sciences, Lanzhou 730000, China*

^c*RIKEN BNL Research center, Brookhaven National Laboratory, Upton, NY, 11973, USA*

We present lattice QCD results for masses and magnetic polarizabilities of light and strange pseudo-scalar mesons, chiral condensates, decay constants of neutral pion and neutral kaon in the presence of background magnetic fields with eB ranging up to around 3.35 GeV^2 ($\sim 70 M_\pi^2$) in the vacuum. The computations were carried out in (2+1)-flavor QCD on $32^3 \times 96$ lattices using the Highly Improved Staggered Quarks (HISQ) action with $M_\pi \approx 220 \text{ MeV}$ at zero temperature. We find that the masses of neutral pseudo-scalar mesons monotonously decrease as the magnetic field strength grows and then saturate at a nonzero value, while there exists a non-monotonous behavior of charged pion and kaon masses in the magnetic field. We observe a qB scaling of the up and down quark flavor components of neutral pion mass, neutral pion decay constant as well as the quark chiral condensates at $0.05 \lesssim eB \lesssim 3.35 \text{ GeV}^2$. We show that the next-to-leading order chiral correction to the Gell-Mann-Oakes-Renner relation involving neutral pion is less than 6% and the correction for the relation involving neutral kaon is in the range of (56-72)% at $eB \lesssim 3.35 \text{ GeV}^2$. We also derive the Ward-Takahashi identities for QCD in the magnetic field in the continuum formulation including the relation between neutral pseudo-scalar meson correlators and chiral condensates.

I. INTRODUCTION

The properties of strong interacting matter in the external magnetic field have attracted a lot of studies in the recent years as strong magnetic fields appear in heavy-ion collisions [1–3], and early universe [4] and magnet stars [5]. The QCD thermodynamics in the presence of a background magnetic field is of particular interest. At zero temperature it is found from lattice QCD studies using standard staggered fermions that the order parameter of the transition, chiral condensate, increases with the magnetic field strength eB (so-called magnetic catalysis) [6, 7]. This suggests that the magnitude of the chiral symmetry breaking becomes larger in the vacuum which leads to an expectation that the chiral crossover transition temperature T_{pc} increases with the magnetic field strength eB , which is also seen in the lattice QCD studies in 2-flavor and 3-flavor QCD using standard staggered fermions at finite lattice cutoffs [6, 8]. However, surprise came later that T_{pc} actually decreases with eB as found from continuum extrapolated results in $N_f = 2 + 1$ lattice QCD studies using improved staggered (stout) fermions [9]. The discrepancy of results in Ref. [6] from those in Ref. [9] is most likely due to the large discretization errors in the standard staggered fermions [8]. Accompanying the reduction of T_{pc} a decreasing behavior of chiral condensate in eB in the proximity of transition temperature, i.e. the so-called inverse magnetic catalysis (IMC) is also found in Ref. [9, 10] and further lattice QCD studies using improved discretization schemes [11–14]. Many model and theoretical studies have been performed to understand the (inverse) magnetic catalysis, reduction of T_{pc} as well as their relations [7, 15–26]. Recently it has been suggested from lattice QCD studies that the IMC is not necessarily associated with the reduction of T_{pc} as a function of eB by performing simulations with heavier-than-physical pions [27, 28] and it is more like a deconfinement catalysis [29].

Although the increase (reduction) of T_{pc} is often connected with the increase (reduction) of chiral condensates, which suggests the increase (reduction) of the magnitude of the chiral symmetry breaking, the breaking of chiral symmetry in QCD is also related to the Goldstone pions. At vanishing magnetic field the square of the Goldstone pion mass is proportional to the product of a sum of quark masses and quark condensates, where the former explicitly breaks the chiral symmetry of the QCD Lagrangian, the latter measures the strength of spontaneous symmetry breaking. This is the well-known Gell-Mann-Oakes-Renner (GMOR) relation [30], and the validity of GMOR the relation has been confirmed on lattice QCD simulations at vanishing magnetic field and in the vacuum [31]. The GMOR relation has also been extended to the 3-flavor case including a strange quark [32], and the next-to-leading order chiral corrections to the GMOR relation have also been studied at zero temperature and vanishing magnetic field [33–35]. Extending to the case of low temperature and vanishing magnetic field [36], weak magnetic field at zero temperature [37] and in both low temperature and weak magnetic field [38] it is found that the GMOR relation for neutral pions holds true in the leading order chiral perturbation theory (χ PT) in the chiral limit of quark masses as well. As it is known that at vanishing magnetic field the transition temperature decreases with lighter pions [39, 40] one may expect that the reduction of the transition temperature in the magnetic field could be associated with a lighter Goldstone boson which can be a neutral pion.

Meson spectrum of QCD in the external magnetic field is of important interest by itself [16, 26, 41–47], and in particular the mass of a neutral pion in the external magnetic field may be helpful to understand the reduction of T_{pc}

given that neutral pion is a Goldstone boson in the nonzero magnetic field. Besides that as implied from the QCD inequality [48] the mass sum of the up and down quark flavor components of the neutral pion is a lower bound of the mass of a charged ρ meson whose condensation could signal the transition of the QCD vacuum into a superconducting state in a sufficiently strong magnetic field [49, 50]. Most of lattice studies on the meson spectrum in external magnetic fields have been performed in the quenched approximation, e.g. in the quenched two color QCD with overlap fermions as valence quarks [51], quenched QCD with Wilson fermions [48, 52] and overlap fermions [53, 54] as valence quarks in the computation of meson correlation functions. In the earlier studies there exists a discrepancy in the behavior eB dependence of the neutral pion mass from lattice QCD studies in the quenched approximation, i.e. for quenched unimproved Wilson fermions the neutral meson mass firstly decreases and then increases as eB grows [48] while for quenched overlap fermions it monotonously decreases [53]. Later the discrepancy is resolved as pointed out in Ref. [52] that the eB -dependence of hopping parameter κ has to be taken into account in the discretization scheme using Wilson fermions, and a monotonous reduction of neutral pion mass with increasing eB is finally established in the quenched QCD [52]. While for the case of a charged pion a monotonous increasing of its mass M_{π^-} with eB is found in all the quenched QCD studies [48, 52–54]. On the other hand, lattice studies in full QCD on eB dependence of mass spectrum focus only on the light pseudo-scalar mesons ($\pi^{0,\pm}$) [9, 52]. It is shown in Ref. [9, 52] that behavior of masses of π^0 and π^\pm in external magnetic fields obtained from (2+1)-flavor QCD using stout fermions have similar trends as those from quenched QCD [52–54]. And it is worth mentioning that there exists a possible decreasing trend of charged pion mass in the very strong magnetic field in both quenched [54] and full QCD [9].

Similar decreasing trend of the neutral pion mass and T_{pc} in the nonzero magnetic field shown in [52] might indicate the connection between these two quantities given that the GMOR relation holds in the nonzero magnetic field. However, it is not known yet whether the GMOR relation holds in a strong magnetic field although χ PT suggests its validity in the weak magnetic field. Model studies on the other hand suggest that the GMOR relation holds for neutral chiral pions at nonzero magnetic field while they are violated for the charged ones at $eB \gtrsim 0.2$ GeV² [55]. Studies on the GMOR relation in the nonzero magnetic field are intricate due to the explicit breaking of rational invariance caused by the magnetic field [56]. Investigations on the charge pion decay constant have been performed on the lattice [57] and it was found that a further pion decay constant exists due to the possibility of a nonzero pion-to-vacuum transition via the vector piece of the electroweak current. Both charged and neutral pion decay constants have been parameterized for the one-pion-to-vacuum matrix elements of the vector and axial vector hadronic currents in the background magnetic fields [58] and studied in the NJL model [44, 59]. It is worth noting that early studies on pion decay constants in e.g. Refs. [37, 38, 55, 60] involves only the one for neutral pion fields related to the axial vector current that is parallel to the magnetic field.

In this paper we focus on the chiral properties of QCD vacuum by studying the light and strange meson masses in the pseudo-scalar channel, chiral condensates as well as the neutral pion and kaon decay constants related to the axial vector current in a wide range of magnetic field strength from 0 to ~ 3.35 GeV² in $N_f = 2 + 1$ QCD. We will present a first lattice QCD study on the GMOR relation in the external magnetic field, and show a first observation of qB scaling of up and down quark flavor components of neutral pion mass, neutral pion decay constant and chiral condensates, and discuss the magnetic polarizabilities of light and strange pseudo-scalar mesons. Our lattice simulations are performed on $32^3 \times 96$ lattices at a single lattice cutoff $a = 0.117$ fm using Highly Improved Staggered fermions with a heavier-than-physical pion mass of ~ 220 MeV at zero temperature.

The paper is organized as follows. In Section II we introduce basic quantities we are going to study, in Section III we will describe our simulation parameters in lattice QCD, our methodology to extract the meson masses and the amplitude to compute the decay constants as well as the discussion on the $\pi - \rho$ mixing in the magnetic field via the generalized Ward-Takahashi identities, and in Section IV we will show our results on masses of pseudo-scalar mesons, magnetic polarizabilities, chiral condensates, neutral pion and kaon decay constants as well as corrections to the GMOR relation as a function of the magnetic field strength. Finally we will summarize in Section V. In Appendix A we will show the extended Ward-Takahashi identities in the nonzero magnetic field and in Appendix B we will show the details of the implementation of the magnetic field in the lattice QCD simulations using the Highly Improved Staggered fermions. Some of previous results on the masses of pseudo-scalar mesons have been reported in conference proceedings [61].

II. TEMPORAL CORRELATORS, MASSES OF PSEUDO-SCALAR MESONS, CHIRAL CONDENSATES AND NEUTRAL PION AND KAON DECAY CONSTANTS

Hadron spectrum in the vacuum can be extracted from two-point temporal correlation functions in the Euclidean space

$$G(\tau) = \int d^3\vec{x} \left\langle \mathcal{M}(\vec{x}, \tau) \left(\mathcal{M}(\vec{0}, 0) \right)^\dagger \right\rangle, \quad (1)$$

where $\mathcal{M} = \bar{\psi}(\tau, \vec{x}) \Gamma \psi(\tau, \vec{x})$ is a meson operator that projects to a certain quantum channel $\Gamma = \Gamma_D \otimes t^a$ with Dirac matrices Γ_D and a flavor matrix t^a , and for instance $\Gamma = \gamma_5$ and γ_μ correspond to the pseudo-scalar and vector channel, respectively. The angular brackets $\langle \dots \rangle$ stand for the expectation value over the gauge field ensembles. The temporal correlator decays exponentially at large distance τ

$$\lim_{\tau \rightarrow \infty} G(\tau) \sim e^{-m_\Gamma \tau}, \quad (2)$$

which defines the mass m_Γ of the corresponding ground state. In the case of staggered fermions the corresponding meson operators are of the form $\bar{\psi}(\vec{x})(\Gamma_D \otimes \Gamma_T^*)\psi(x)$ with $\psi(x)$ a 16-component hypercubic spinor and Γ_D and Γ_T Dirac matrices in spin and taste space, respectively. Here we consider local operator only and the meson operator reduces to $\mathcal{M} = \zeta(\vec{x})\bar{\chi}(\vec{x})\chi(\vec{x})$, where $\zeta(x)$ is the phase factor depending on the choice of $\Gamma = \Gamma_D = \Gamma_T$ and $\chi(\vec{x})$ is the staggered fermion field.

The connected part of correlation function of staggered bilinear can thus be written as

$$G(\tau) = - \sum_{x,y,z} \zeta(\vec{n}) \text{Tr} \left[\left(M^{-1}(\vec{x}, \tau; \vec{0}, 0) \right)^\dagger M^{-1}(\vec{x}, \tau; \vec{0}, 0) \right], \quad (3)$$

where $M^{-1}(\vec{x}, \tau; \vec{0}, 0)$ is the staggered propagator from $(\vec{0}, 0)$ to (\vec{x}, τ) . In this work we focus on the mesons in the pseudo-scalar channel built from $\bar{q}_i q_j$ flavor combinations, here $i, j = u, d, s$, and the phase factor for the pseudo-scalar channel is $\zeta(\vec{n}) = 1$. Due to the presence of the magnetic field the iso-spin symmetry of up and down quarks is broken by their different electric charges. The neutral pion thus is not an iso-vector state any more and a full computation of neutral pion correlation function thus involves both connected and disconnected parts of the correlation function as well as the mixing factor between $u\bar{u}$ (π_u^0) and $d\bar{d}$ (π_d^0) components¹. It has been shown in Ref. [54] that the quark-line disconnected part is negligible in the nonzero magnetic fields, and in our current study of neutral pions we thus neglect the disconnected contributions.

A typical staggered meson correlator, for a fixed separation (in lattice unit) between the source and sink, is an oscillating correlator that simultaneously couples to two sets of mesons with the same spin but with opposite parities, and it thus can be parameterized as [62]

$$G(n_\tau) = \sum_{i=1}^{N_{nosc}} A_{nosc,i} \exp(-M_{nosc,i} n_\tau) - (-1)^{n_\tau} \sum_{i=0}^{N_{osc}} A_{osc,i} \exp(-M_{osc,i} n_\tau), \quad (4)$$

where N_{nosc} (N_{osc}) is the number of non-oscillating (oscillating) meson states whose masses are denoted by $M_{nosc,i}$ and $M_{osc,i}$, and $n_\tau = \tau/a \in \mathbb{Z}$ and a is the lattice spacing. Note that both amplitudes, $A_{nosc,i}$ and $A_{osc,i}$ are positive. In the current study the mass M_{nosc} is the mass of pseudo-scalar meson we are interested in.

It is well known that the energy of a point-like charged particle in the nonzero magnetic field and at zero temperature are the Landau levels,

$$E_n^2 = M^2 + (2n+1)|eB| - g s_z qB + p_z^2, \quad n \in \mathbb{Z}_0^+, \quad (5)$$

where M is the mass of a charged particle at zero magnetic field, q is the electrical charge of the particle, s_z is the spin polarization in the z direction and the magnetic field is assumed to go along with the z direction. For pseudo-scalar mesons the gyromagnetic ratio $g = 0$ while for vector mesons $g = 2$. In the case of the lowest Landau level and zero momentum along the z direction, i.e. $n=0$ and $p_z=0$, the mass of a charged point-like pseudo-scalar meson in the external magnetic fields can be expressed as

$$M_{ps}^\pm(B) = \sqrt{(M_{ps}^\pm(B=0))^2 + |eB|}. \quad (6)$$

While the charged particles become heavier with increasing eB , the neutral particle is supposed to remain independent of magnetic field if it remains as a point-like particle. The lightest pseudo-scalar mesons, i.e. pions are of particular interests as which are Goldstone bosons at vanishing magnetic field, and their masses are connected to the quark chiral condensate in the vacuum known as the Gell-Mann-Oakes-Renner relation expressed as [30]

$$(m_u + m_d) (\langle \bar{\psi}\psi \rangle_u + \langle \bar{\psi}\psi \rangle_d) = 2f_\pi^2 M_\pi^2 (1 - \delta_\pi), \quad (7)$$

¹ In the presence of magnetic field the operator for π^0 should be $\alpha \bar{u}\gamma_5 u - \beta \bar{d}\gamma_5 d$ with $\alpha^2 + \beta^2 = 1$ [57]. Here in our computation for the neutral pion correlation function to extract the mass of π^0 and neutral pion decay constant f_{π^0} we have $\alpha = \beta = 1/\sqrt{2}$ as the case for the vanishing magnetic field.

and the above GMOR relation in the two-flavor theory has been extended to the 3-flavor case including a strange quark as follows [32]

$$(m_s + m_d) (\langle \bar{\psi}\psi \rangle_s + \langle \bar{\psi}\psi \rangle_d) = 2f_K^2 M_K^2 (1 - \delta_K), \quad (8)$$

where m_π and m_K are the masses of pion and kaon respectively, f_π (f_K) is the pion (kaon) decay constant, $m_{f=u,d,s}$ is the mass of a up, down and strange quark and the corresponding quark chiral condensate is denoted by $\langle \bar{\psi}\psi \rangle_{f=u,d,s}$. Here in our study of $N_f = 2 + 1$ QCD, $m_u = m_d$ and $m_s/m_l = 10$, and the single flavor quark chiral condensate $\langle \bar{\psi}\psi \rangle_f$ is obtained as follows

$$\langle \bar{\psi}\psi \rangle_f = \frac{1}{4} \frac{1}{V} \frac{\partial \ln Z}{\partial m_f} = \frac{1}{4} \frac{1}{V} \text{Tr} D_f^{-1}, \quad (9)$$

where Z is the partition function of QCD, V is the full volume of space-time, and the factor $1/4$ accounts for the fourth root of Dirac matrix D_f in the staggered theory. δ_π and δ_K are the next-to-leading order chiral corrections, and both of them are related with some low-energy constants and have a relation of $\delta_K = M_K^2/M_\pi^2 \delta_\pi$ [32]. The estimates on these two quantities using χ PT combining with QCD sum rules are $\delta_\pi = (6.2 \pm 1.6)\%$ and $\delta_K = (55 \pm 5)\%$ at the physical mass point and vanishing magnetic field [34, 35].

As mentioned in the introduction, some additional pion decay constants related to the vector and axial vector currents can be defined in the external magnetic fields [56–58], here in the current paper we restrict ourselves focusing on the original neutral pion and kaon decay constants which are related only to the axial vector current associated with the direction parallel to the magnetic field at zero momentum. This decay constant has the same definition as that at vanishing magnetic field [56, 58, 63], which is written as follows

$$\sqrt{2} f_{\pi^0} M_{\pi^0}^2 = (m_u + m_d) \left\langle 0 \left| \frac{1}{\sqrt{2}} (\bar{u}\gamma_5 u - \bar{d}\gamma_5 d) \right| \pi^0(\mathbf{p} = 0) \right\rangle, \quad (10)$$

$$\sqrt{2} f_{K^0} M_{K^0}^2 = (m_d + m_s) \langle 0 | \bar{d}\gamma_5 s | K^0(\mathbf{p} = 0) \rangle. \quad (11)$$

We will also look into the up and down quark flavor components of the neutral pion decay constant ($f_{\pi_u^0}$ and $f_{\pi_d^0}$) and neutral pion mass ($m_{\pi_u^0}$ and $m_{\pi_d^0}$), whose relation is expressed as follows

$$\sqrt{2} f_{\pi_u^0} M_{\pi_u^0}^2 = 2m_u \langle 0 | \bar{u}\gamma_5 u | \pi_u^0(\mathbf{p} = 0) \rangle, \quad (12)$$

$$\sqrt{2} f_{\pi_d^0} M_{\pi_d^0}^2 = 2m_d \langle 0 | \bar{d}\gamma_5 d | \pi_d^0(\mathbf{p} = 0) \rangle. \quad (13)$$

The corresponding GMOR relation is thus

$$4m_u \langle \bar{\psi}\psi \rangle_u = 2f_{\pi_u^0}^2 M_{\pi_u^0}^2 (1 - \delta_{\pi_u^0}), \quad (14)$$

$$4m_d \langle \bar{\psi}\psi \rangle_d = 2f_{\pi_d^0}^2 M_{\pi_d^0}^2 (1 - \delta_{\pi_d^0}). \quad (15)$$

The matrix elements in Eqs. 10, 11, 12 and 13 can be extracted from the correlation function of pseudo-scalar meson at zero spatial momentum $\langle O_S(\tau) P_W(0) \rangle$ [64]. The amplitude of the correlation function can be written as

$$C_{O_S P_W} = \frac{\langle 0 | O_S | P(\vec{p} = 0) \rangle \langle P(\vec{p} = 0) | P_W | 0 \rangle}{2M_P V_s}, \quad (16)$$

where V_s is the spatial lattice volume, P denotes the operator for π^0 , K and $\pi_{u,d}^0$ with M_P the corresponding meson masses. By inserting the corresponding operator ($O_S = P_W$) into Eq. 16 and combining Eqs. 10, 11, 12 and 13, the pion and kaon decay constants can be obtained as follows [64]

$$f_{P^\pi} = 2m_l \sqrt{\frac{V_s}{4}} \sqrt{\frac{C_{P_W^\pi P_W^\pi}}{M_{P^\pi}^3}}, \quad (17)$$

$$f_{K^0} = (m_d + m_s) \sqrt{\frac{V_s}{4}} \sqrt{\frac{C_{K_W^0 K_W^0}}{M_{K^0}^3}}, \quad (18)$$

where a factor of $1/\sqrt{4}$ on the right hand sides of the above equations accounts for the case in staggered fermions, $m_l = m_u = m_d$, and P^π denotes the cases for π^0 , π_u^0 and π_d^0 . The amplitudes $C_{P_W^\pi P_W^\pi}$ and $C_{K_W^0 K_W^0}$ as well as the masses M_{P^π} and M_{K^0} will be obtained from the mass fit (cf. Eq. 4) to the correlators in the pseudo-scalar channel.

III. NUMERICAL SETUPS

A. Lattice setup

Most of previous lattice QCD studies for $(2 + 1)$ -flavor QCD in the external magnetic field were performed using the stout staggered fermions. In our current simulations we use $N_f = 2 + 1$ Highly Improved Staggered Quarks (HISQ) [65]. At a given value of the lattice spacing the HISQ action achieves better taste symmetry than 2stout actions [66]. The HISQ action is constructed by the Kogut-Susskind 1-link action and Naik improvement term with smeared links. The smeared links are obtained in the following way. Firstly level one smeared links V_μ are constructed by fat-7 from thin SU(3) links U_μ . Next, re-unitarized links W_μ are constructed by projecting V_μ on $U(3)$. Finally, level two smeared links X_μ are constructed by fat-7 from thin SU(3) links W_μ with the Lepage term. The HISQ Dirac operator are built by the Kogut-Susskind term with X_μ and the Naik term with W_μ . The magnetic field only couples directly to quarks thus the implementation of magnetic field is done just by replacing $X_\mu \rightarrow u_\mu X_\mu$ in the Kogut-Susskind term and $W_\mu \rightarrow u_\mu W_\mu$ in the Naik term [14]. Details about the implementation of magnetic fields in the lattice QCD simulations using the HISQ action are summarized in Appendix B.

The external magnetic field pointing along the z -direction $\vec{B} = (0, 0, B)$ is described by a fixed link variable $u_\mu(n)$ of the $U(1)$ field, and $u_\mu(n)$ is expressed as follows in the Landau gauge [9, 67],

$$\begin{aligned} u_x(n_x, n_y, n_z, n_\tau) &= \begin{cases} \exp[-iqa^2BN_xn_y] & (n_x = N_x - 1) \\ 1 & (\text{otherwise}) \end{cases} \\ u_y(n_x, n_y, n_z, n_\tau) &= \exp[iqa^2Bn_x], \\ u_z(n_x, n_y, n_z, n_\tau) &= u_t(n_x, n_y, n_z, n_\tau) = 1. \end{aligned} \quad (19)$$

Here the lattice size is denoted as (N_x, N_y, N_z, N_τ) and coordinates as $n_\mu = 0, \dots, N_\mu - 1$ ($\mu = x, y, z, \tau$). The external magnetic field applied along the z -direction $\mathbf{B} = (0, 0, B)$ is quantized in the following way

$$qB = \frac{2\pi N_b}{N_x N_y} a^{-2}, \quad (20)$$

where q is the electric charge of a quark, and N_x (N_y) is the number of points in the x (y) direction on the lattice. Since the quantization has to be satisfied for all the quarks in the system, a greatest common divisor of the electric charge for all the quarks, i.e. $|q_d| = |q_s| = e/3$ with e the elementary electric charge, is chosen in our simulation. Thus the strength of the magnetic field eB practically is expressed as follows

$$eB = \frac{6\pi N_b}{N_x N_y} a^{-2}, \quad (21)$$

where $N_b \in \mathbf{Z}$ is the number of magnetic flux through unit area in the x - y plane. The periodic boundary condition for $U(1)$ links is applied for all directions except for the x -direction. As limited by the boundary condition N_b is constrained in the range of $0 \leq N_b < \frac{N_x N_y}{4}$.

For the gauge part we use a tree-level improved Symanzik gauge action. The simulations have been performed on $32^3 \times 96$ lattices at zero temperature. The inverse lattice spacing is $a^{-1} \simeq 1.685$ GeV, and strange quark mass m_s is tuned to its physical value by tuning the mass of the η_s^0 meson, $M_{\eta_s^0} \simeq 684$ MeV which is based on the leading order chiral perturbation theory relation $M_{\eta_s^0} = \sqrt{2M_K^2 - M_\pi^2}$ between masses of η_s^0 , π and K . The light quark mass is then set to be $m_l = m_s/10$ corresponding to a pion mass $M_\pi \simeq 220$ MeV in the vacuum. The details on the scale setting can be found in Ref. [62, 68].

In our simulations 16 different values of N_b have been chosen, i.e. 0, 1, 2, 3, 4, 6, 8, 10, 12, 16, 20, 24, 32, 40, 48 and 64 whose corresponding magnetic field strength eB ranges from 0 to around 3.35 GeV². All configurations have been produced using Rational Hybrid Monte Carlo (RHMC) algorithm and are saved by every 5 time units, and the statistics for each N_b is about $O(\sim 10^3)$. Details of eB and statistics are listed in Table I.

B. Meson correlation functions

We show our results of correlation functions for $\pi_u^0 (u\bar{u})$ and $\pi_d^0 (d\bar{d})$ as an example in the left and right plot of Fig. 1, respectively. It can be seen clearly that with increasing magnetic field strength eB both correlation functions become larger, and the $u\bar{u}$ component of the two-point correlation function increases faster. This may be understood

eB [GeV ²]	0	0.052	0.104	0.157	0.209	0.314	0.418	0.523
N_b	0	1	2	3	4	6	8	10
# of conf.	2548	2651	3135	2444	2224	3142	2935	3302
eB [GeV ²]	0.627	0.836	1.045	1.255	1.673	2.09	2.510	3.345
N_b	12	16	20	24	32	40	48	64
# of conf.	3432	1993	3160	1994	2174	3385	2234	3263

TABLE I. The statistics of analyzed $32^3 \times 96$ lattices with $\beta = 6.68$ and $a \simeq 0.117$ fm ($a^{-1} \simeq 1.685$ GeV) produced using the HISQ fermion action and a tree-level improved Symanzik gauge action in $N_f = 2 + 1$ QCD. The pion mass used in the simulation is tuned to be 220 MeV, obtained mass of ρ is $M_\rho = 779(35)$ MeV, $M_K = 507.03(7)$ MeV and $M_{\eta_s} = 684.44(6)$ MeV at $eB = 0$.

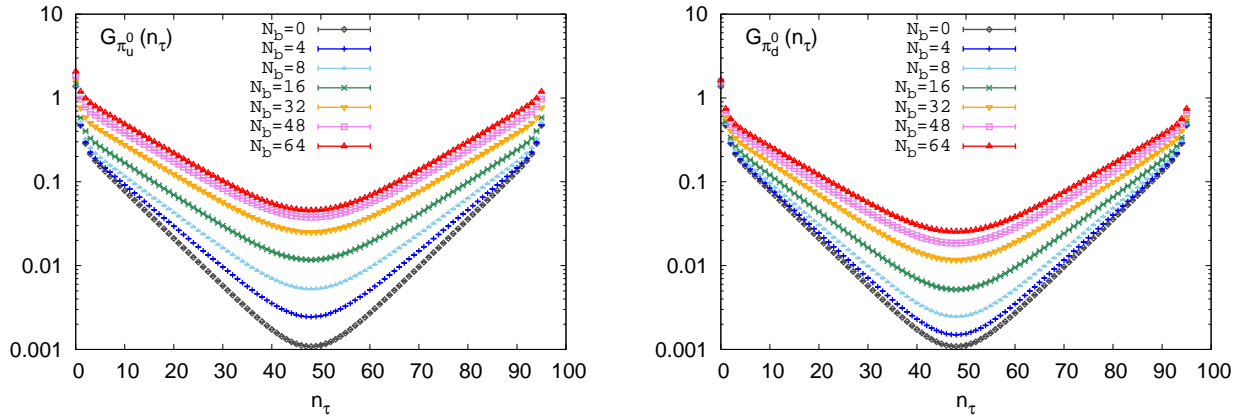


FIG. 1. Left: The $u\bar{u}$ component of the neutral pion correlation function $G_{\pi_u^0}(n_\tau)$ at different values of N_b calculated using 12 corner wall sources. Right: Same as left one but for the $d\bar{d}$ component $G_{\pi_d^0}(n_\tau)$. G shown here are rescaled with lattice spacing a such that they are dimensionless quantities.

that the internal structure of pion is probed and the $u\bar{u}$ component is more affected due to the larger absolute value of electrical charge of the u quark.

We then extract the mass of neutral as well as the charged pseudo-scalar mesons by fitting to the corresponding temporal correlation functions with the ansatz (cf. Eq. 4). The non-oscillating states are the physical states we need, and oscillating states are also necessary to be included in the fit in particular in the case to correlation functions for charged particles. In the fits we used various numbers of non-oscillating as well as oscillating states, i.e. (N_{nosc}, N_{osc}) has been set to $(1,0)$, $(1,1)$, $(2,1)$. All the fits have been performed in a given interval $[\tau_{min}, N_\tau/2]$, where τ_{min} ranges from 0 to $N_\tau/2 - 1$. The final results are chosen as the best fit from all different fit modes through the AICc (corrected Akaike Information criterion) [69, 70]

$$\text{AICc} = 2k - \ln(\hat{L}) + \frac{2k^2 + 2k}{n - k - 1}, \quad (22)$$

where k is the number of parameters, \hat{L} is the likelihood function, and the last term is needed to correct over-fitting if the number of data points n is not much larger than k . Then we choose a plateau in the AICc selected results and obtain the final mass and its uncertainty from the plateau by using a Gaussian bootstrapping method [62].

Since correlation functions computed using a single point source do not suppress the excited states and make the extraction of ground states difficult we thus also compute correlation functions using a corner wall source which means putting an unit source at the origin of each 2^3 on a chosen z -slice [62, 71–73]. We further improve the signal by putting 12 corner wall sources at $(0,0,0,0)$, $(0,0,0,8)$, ..., $(0,0,0,88)$. The signal-to-noise ratio $\delta G(\tau)/\langle G(\tau) \rangle$ obtained using a single corner wall source is reduced by a factor of 6 compared to the results obtained using a single point source. The signal-to-noise ratio obtained using multiple corner wall sources is found $\sqrt{\# \text{ of sources}}$ times better than using a single corner wall source. We provide a typical example of the fit results, whose procedure was illustrated earlier, for the $u\bar{u}$ component of a neutral pion correlation function at $eB=0.84$ GeV² measured using a single point source (top two plots) and 12 corner wall sources (bottom two plots) in Fig. 2. We find that the usage of corner wall sources

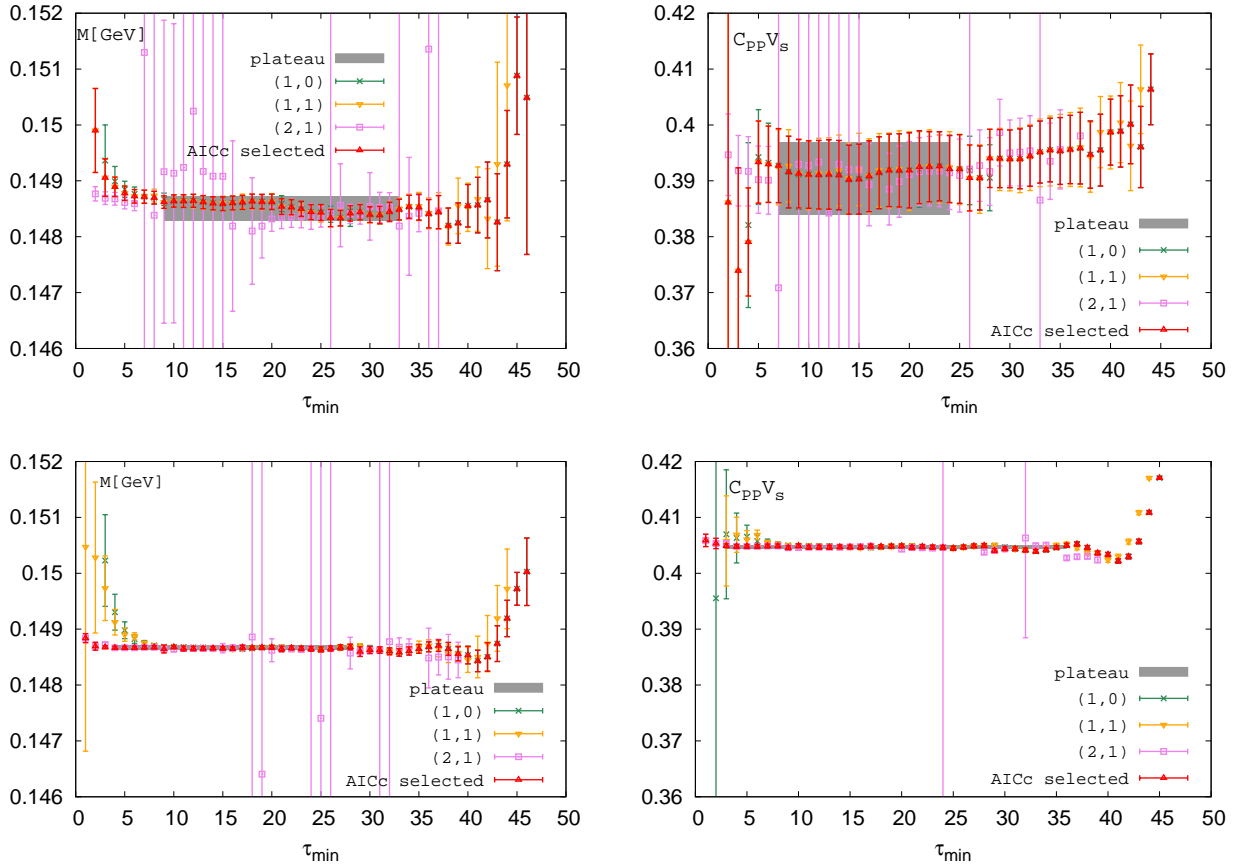


FIG. 2. Top: Mass (left) and its associated matrix element C_{PP} multiplied by the spatial volume V_s (right) of π_u^0 at $N_b = 16$ ($eB = 0.84 \text{ GeV}^2$) with these different fit modes: (# of non-oscillating states, # of oscillating states) = (1,0), (1,1), (2,1) obtained from the fits to correlation functions measured using a single point source. Bottom: Same as the top two plots but for fits to correlation functions measured using 12 corner wall sources.

yields a much better signal in the ground states as compared to that of the point source and has a longer plateau with much smaller uncertainty. The value of ground state mass extracted using the corner wall source is consistent within that extracted using the point source. As seen from Fig. 2 the corner wall source also works better for the extraction of the amplitude in the same way, i.e. the amplitude obtained with corner wall source is about 3% larger than the amplitude obtained with point source while the relative error is reduced by ~ 20 times. The amplitude obtained from the corner wall sources is then used in the calculation of decay constants in Section IV.

C. Mixing of pion states and Ward-Takahashi identities at $eB > 0$

Since the states of vector meson ρ with spin polarization $s_z = 0$, i.e. $\rho_{s_z=0}$ has the same quantum number of the states of π in the presence of magnetic field it is supposed that the mixing between the pion and $\rho_{s_z=0}$ states is enabled [52], i.e. neutral π^0 mixes with neutral $\rho_{s_z=0}^0$ while charged π^\pm mixes with charged $\rho_{s_z=0}^\pm$.² This is to say that once the mixing is enabled correlation functions in the vector channel and pseudo-scalar channels receive mutual contributions and their corresponding ground state masses should be the same. The mixing has been investigated in details in quenched QCD in Ref. [52], and it was found that the influence to the ground state of π is negligible. Here we show another evidence that the influence of mixing to neutral pseudo-scalar meson states is mild by looking into

² Note that the mixing with $s_z = \pm 1$ is not permitted due to the conservation of angular momentum.

the following Ward-Takahashi identities (cf. A.31, A.32 and A.33 in Appendix A 2)

$$\langle \bar{\psi}\psi \rangle_f = m_f \chi_{\text{ps}_f^0}, \quad (23)$$

$$\langle \bar{\psi}\psi \rangle_d + \langle \bar{\psi}\psi \rangle_s = (m_d + m_s) \chi_{K^0}, \quad (24)$$

where $\chi_{\text{ps}_f^0}$ is the space-time sum of the correlation function of neutral mesons consisting only $f\bar{f}$ in the pseudo-scalar channel, $\chi_{\text{ps}_f^0} = \sum_{\tau=0}^{N\tau-1} G_{\text{ps}}(\tau)$ with $f = u, d$ and s quark flavors. This is to say that $\chi_{\text{ps}_f^0}$ is evaluated by using the $u\bar{u}$, $d\bar{d}$ and $s\bar{s}$ components of the correlation functions of neutral pseudo-scalar mesons, i.e. π_u^0 , π_d^0 and η_s^0 . The chiral condensate $\langle \bar{\psi}\psi \rangle_f$ with the corresponding flavor is computed via Eq. 9. And χ_{K^0} is the space-time sum of the neutral kaon correlators. As shown in Appendix A.32 and A.31 the above Eq. 23 for $f = s$ should hold at nonzero magnetic field, while for neutral pion we only look the connected part and break it into the up and down quark flavor components, i.e. for $f = u$ and d , respectively. The ratio of $\langle \bar{\psi}\psi \rangle_f / (m_f \chi_{\text{ps}_f^0})$ ($f = u, d, s$) as a function of eB is shown in the left plot of Fig. 3. We found that all the ratios agree with unity with deviations less than 1.2% at all the values of magnetic field strength we studied and this indicates that the influence of the mixing to neutral pseudo-scalar states is negligible. The other indication is that for the neutral pion the mixing between $\bar{u}\gamma_5$ and $\bar{d}\gamma_5$ stays almost the same as they were at zero magnetic field. Results for the ratio of left hand side to right hand side of Eq. 24 as derived in Appendix A 2 are shown in the right plot of Fig. 3, and the deviation from unity is less than 0.6% in $eB \in [0, 3.35]$ GeV^2 .

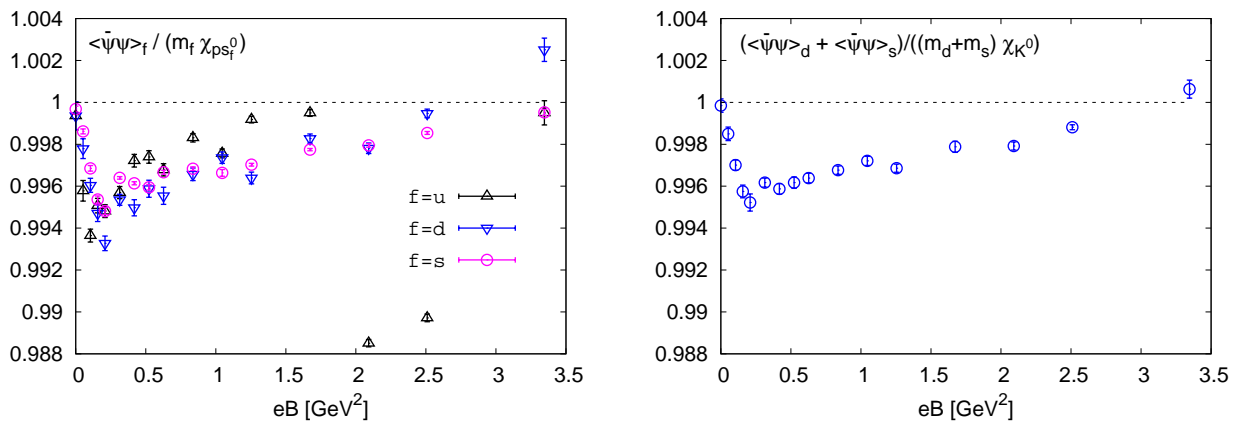


FIG. 3. Left: Ratio of $\langle \bar{\psi}\psi \rangle_f / (m_f \chi_{\text{ps}_f^0})$ as a function of eB for f as up (u), down (d) and strange (s) quark flavors. Right: Ratio of $(\langle \bar{\psi}\psi \rangle_d + \langle \bar{\psi}\psi \rangle_s) / ((m_d + m_s) \chi_{K^0})$ as a function of eB .

D. UV divergence of quark chiral condensates

To investigate the GMOR relation we need to take care of the UV divergence in the light and strange quark chiral condensates at zero and nonzero magnetic field. Since it has been shown in Ref. [9] that the UV divergence part of the chiral condensate is independent of the magnetic field, we can obtain the UV-free chiral condensate at nonzero magnetic field by subtracting the UV-divergence in the chiral condensate, i.e. $\langle \bar{\psi}\psi \rangle_{f=l,s}^{\text{UV}}$ obtained at the zero magnetic field. To obtain $\langle \bar{\psi}\psi \rangle_{l,s}^{\text{UV}}$ we thus look into the Dirac spectrum representation of the subtracted chiral condensate at zero magnetic field,

$$\langle \bar{\psi}\psi \rangle_{\text{sub}} \equiv \langle \bar{\psi}\psi \rangle_l - \frac{m_l}{m_s} \langle \bar{\psi}\psi \rangle_s = \int_0^\infty \frac{2m_l(m_s^2 - m_l^2)\rho(\lambda)}{(\lambda^2 + m_l^2)(\lambda^2 + m_s^2)} d\lambda, \quad (25)$$

where $\rho(\lambda)$ is the eigenvalue spectral density of fermion matrix D_f (cf. Eq. 9), and the light (up or down) quark and strange quark chiral condensate, $\langle \bar{\psi}\psi \rangle_l$ and $\langle \bar{\psi}\psi \rangle_s$, are connected to $\rho(\lambda)$ through the following relation

$$\langle \bar{\psi}\psi \rangle_{l,s} = \int_0^\infty \frac{2m_{l,s}\rho(\lambda)}{\lambda^2 + m_{l,s}^2} d\lambda. \quad (26)$$

The UV divergence part of the quark chiral condensate that is linear in quark mass is thus absent in $\langle\bar{\psi}\psi\rangle_{sub}$, while a logarithm UV divergence in the light quark chiral condensate should be negligible. Thanks to the Chebyshev filtering technique combined with the stochastic estimate method [14, 74–77] we are able to compute the complete Dirac eigenvalue spectrum $\rho(\lambda)$ and then reproduce $\langle\bar{\psi}\psi\rangle_{sub}$ as well as $\langle\bar{\psi}\psi\rangle_l$ and $\langle\bar{\psi}\psi\rangle_s$ through Eqs. 25 and 26, respectively³. In the Dirac eigenvalue spectrum the UV divergence part should be represented by $\rho(\lambda)$ with $\lambda \geq \lambda_{cut}^{UV}$. Thus the UV divergence part of light quark condensate can be expressed as

$$\langle\bar{\psi}\psi\rangle_{l,s}^{UV} = \int_{\lambda_{cut}^{UV}}^{\infty} \frac{2 m_{l,s} \rho(\lambda)}{\lambda^2 + m_{l,s}^2} d\lambda. \quad (27)$$

Given that the logarithm divergence in quark mass is negligible the UV-divergence part in the strange quark chiral

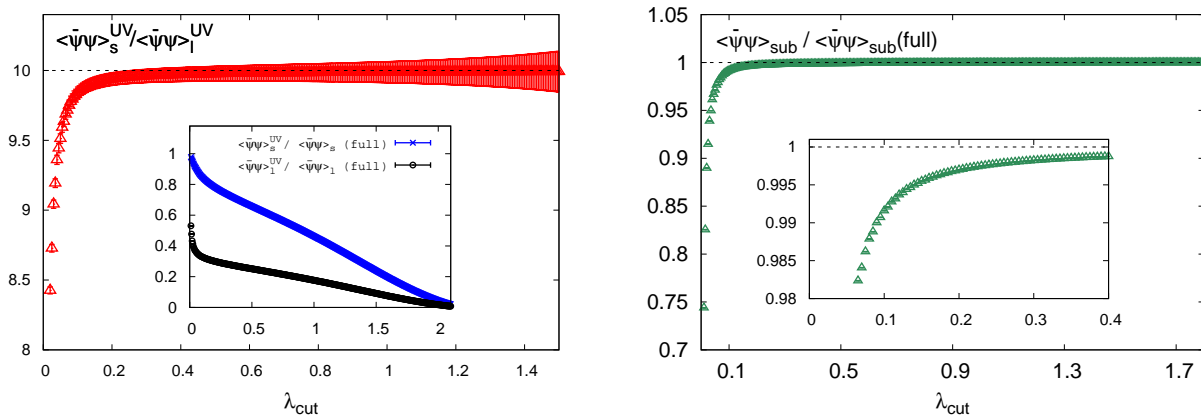


FIG. 4. Left: Ratio of $\langle\bar{\psi}\psi\rangle_s^{UV} / \langle\bar{\psi}\psi\rangle_l^{UV}$ as a function of λ_{cut} . The inset shows the ratios of $\langle\bar{\psi}\psi\rangle_{l,s}^{UV}$ to the corresponding full quark condensates as a function of λ_{cut} . Right: Ratio of the subtracted chiral condensates with an upper cutoff λ_{cut} in the integration of λ in Eq. 25 to that with a full spectrum of $\rho(\lambda)$ as a function of λ_{cut} . The inset shows a blowup in the y axis region close to 1.

condensate should be m_s/m_l times as that in the light quark chiral condensate, i.e. $\langle\bar{\psi}\psi\rangle_s^{UV} = 10 \langle\bar{\psi}\psi\rangle_l^{UV}$ in our case. Thus $\langle\bar{\psi}\psi\rangle_{l,s}^{UV}$ can be determined with the smallest value of λ_{cut}^{UV} which makes $\langle\bar{\psi}\psi\rangle_s^{UV} / \langle\bar{\psi}\psi\rangle_l^{UV} = 10$.

To determine the value of λ_{cut}^{UV} we show the ratio $\langle\bar{\psi}\psi\rangle_s^{UV} / \langle\bar{\psi}\psi\rangle_l^{UV}$ as a function of λ_{cut} in the left plot of Fig. 4. We see that the ratio approaches 10 rapidly at $\lambda_{cut} \lesssim 0.2$ and then saturate at 10 at larger values of λ_{cut} . We thus pick up a value of 0.24 to be λ_{cut}^{UV} which makes the ratio start to approach 10 by less than 0.5%. As seen from the inset in the left plot of Fig. 4 $\langle\bar{\psi}\psi\rangle_{l,s}^{UV}(\lambda_{cut})$ itself is a rapidly decreasing function of λ_{cut} , we also check the uncertainty in the determination of λ_{cut}^{UV} by looking to the subtracted chiral condensate. We compute $\langle\bar{\psi}\psi\rangle_{sub}(\lambda_{cut})$ as a function of λ_{cut} being the upper bound of the integration variable λ in Eq. 25, and show its ratio to $\langle\bar{\psi}\psi\rangle_{sub}(\lambda_{cut} = \infty)$ as a function λ_{cut} in the right plot of Fig. 4. Thus λ_{cut}^{UV} should be the smallest value of λ_{cut} at which $\langle\bar{\psi}\psi\rangle_{sub}(\lambda_{cut}) / \langle\bar{\psi}\psi\rangle_{sub}(\lambda_{cut} = \infty) \simeq 1$. As seen from the plot the ratio approaches unity at very small values of λ_{cut} , e.g. at $\lambda_{cut} \simeq 0.12$ the ratio is 0.5% deviation from unity.

Since it is not very clear how large the logarithm divergence in quark mass contributes to the UV-divergence in the quark chiral condensates, we adopt a rather wide window for the values of λ_{cut}^{UV} from 0.12 to 0.36 with the central value 0.24 which gives $\langle\bar{\psi}\psi\rangle_s^{UV} / \langle\bar{\psi}\psi\rangle_l^{UV} \simeq 10$. Then the obtained $\langle\bar{\psi}\psi\rangle_l^{UV}$ ranges from about 32% to 27% of $\langle\bar{\psi}\psi\rangle_l$ at $eB = 0$, while $\langle\bar{\psi}\psi\rangle_s^{UV}$ ranges from about 83% to 71% of $\langle\bar{\psi}\psi\rangle_s$ at $eB = 0$.

IV. RESULTS

A. Masses and magnetic dipole polarizabilities of light and strange pseudo-scalar mesons

We now present our results for masses of pseudo-scalar mesons calculated at 16 different values of eB ranging from 0 to $\sim 3.35 \text{ GeV}^2$. In the left plot of Fig. 5 we show the ratio of masses of neutral pseudo-scalar mesons at nonzero

³ With the order of Chebyshev polynomials being 24000 and the binwidth of Dirac eigenvalue spectrum in lattice spacing being 0.002 $\langle\bar{\psi}\psi\rangle_{sub}$, $\langle\bar{\psi}\psi\rangle_l$ and $\langle\bar{\psi}\psi\rangle_s$ obtained from the stochastic noise method (cf. Eq. 9) are reproduced within an accuracy of 1% via Eqs. 25 and 26.

magnetic field to those at zero magnetic field as a function of eB . We found that the masses of all neutral mesons decrease with increasing eB and has a tendency to saturate at $eB \gtrsim 2.5 \text{ GeV}^2$. By comparing the normalized masses of π_u^0 , π_d^0 , K^0 , η_s , it is obvious that the lighter hadrons are more affected by magnetic field, i.e. in the strongest magnetic field ($eB \simeq 3.35 \text{ GeV}^2$) we have it can be seen that M_{η_s} and $M_{\pi_u^0}$ ($M_{\pi_d^0}$) are about 70% and 60% of their values at $B=0$, respectively. The amount of reduction in $\bar{u}u$ and $\bar{d}d$ components of pion mass is roughly consistent with results presented in SU(2) gauge theory [51] and SU(3) quenched QCD [52] as well as in $N_f = 2 + 1$ QCD with stout fermions and physical pion mass in the vacuum [9], while in the former case $M_{\pi_u^0}$ [52] decreases faster while the latter $M_{\pi_u^0}$ [9] decrease slower with eB compared to our current study. This could be partly due to the fact that the hadrons with larger masses are less affected by the magnetic field, as in [52] the pion mass in the vacuum is about 415 MeV, while in [9] it is 135 MeV. Due to the presence of a nonzero magnetic field the $SU_V(2)$ symmetry is broken and mixture of the $u\bar{u}$ and $d\bar{d}$ flavor contents in the neutral pion could depend on eB [52]. To determine the mixture coefficient is beyond the scope of our current paper, and for demonstration we nevertheless show in the left plot of Fig. 5 the ground state mass of π^0 extracted from the averaged correlation functions of $u\bar{u}$ and $d\bar{d}$ in the pseudo-scalar channel, i.e. $G_{\pi^0} = (G_{\pi_u^0} + G_{\pi_d^0})/2$ assuming that the contribution of the disconnected diagram is negligible and the mixture coefficients are the same as the $B = 0$ case [54]. As seen from the plot the ratio for π^0 is in between those for π_u^0 and π_d^0 as expected.

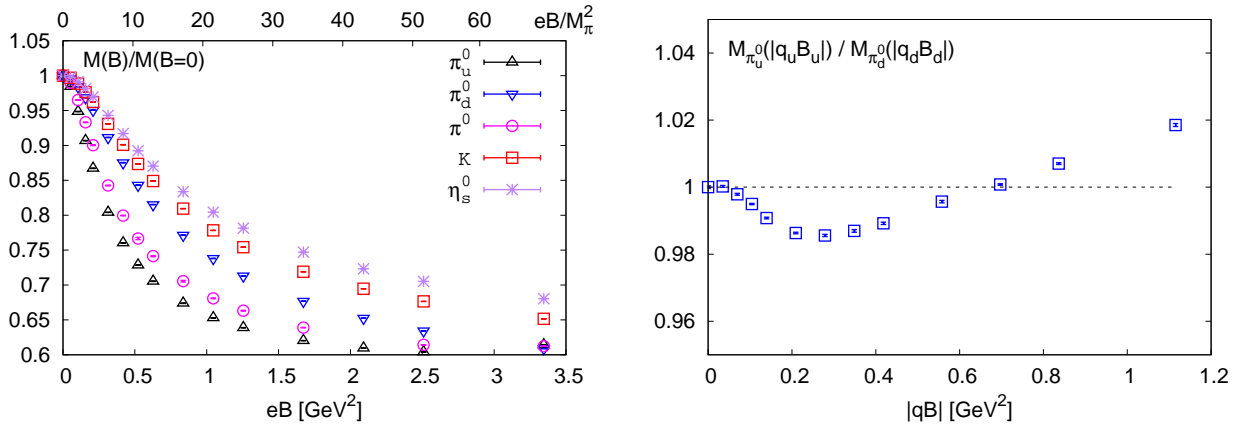


FIG. 5. Left: Masses of π_u^0 , π_d^0 , K , η_s^0 normalized by their corresponding masses at $eB=0$ as a function of eB . Right: Ratio $M_{\pi_u^0}(|q_u B_u|)/M_{\pi_d^0}(|q_d B_d|)$ as a function of $|qB|$. Here q_u and q_d stand for the electrical charges of u and d quarks, and B_u and B_d are different values of B which makes $|qB| \equiv |q_u B_u| = |q_d B_d|$.

Since $M(B)/M(B=0)$ deviates from unity at all the values of eB we simulated the pseudo-scalar mesons studied here thus cannot be considered as neutral point-like particles whose masses should be independent of eB . Also the different magnitudes of the mass reduction between π_u^0 and π_d^0 may come from the different electric charges of up and down quarks which again indicates that the inner structure of meson has been revealed. Since the internal structure of the neutral pion is probed within our current window of magnetic field, we intend to investigate the influence of the electrical charge of quarks on the mass of neutral pion. We thus show the ratio of $M_{\pi_u^0}$ to $M_{\pi_d^0}$ as a function of qB instead of eB in the right plot of Fig. 5. We found for the first time to our knowledge that after rescaling x axis from eB into qB , $M_{\pi_u^0}(|q_u B_u|)$ is almost the same as $M_{\pi_d^0}(|q_d B_d|)$ at $|qB| = |q_u B_u| = |q_d B_d|$ and differs at most by 2%. Here q_u and q_d are the electric charges of u and d quarks, respectively, and $B_{u,d}$ stands for different values of B the quark feels to make $|qB|$ the same for up and down quarks. We call this behavior the qB scaling. This again supports that the internal structure of pions is probed, and may reveal that the dominant degree is represented by the single quark already starting at the smallest magnetic field we simulated, i.e. $eB \approx 0.05 \text{ GeV}^2$. Note that this smallest value of eB is about the value of $M_\pi^2(B=0)$ in our simulation.

We now turn to the case of charged pseudo-scalar mesons, i.e. π^- and K^- , and show the differences of their squared masses from the case of zero magnetic field, i.e. $M^2(eB) - M^2(eB=0)$ in the left plot of Fig. 6⁴. We see that for both π^- and K^- the differences show a non-monotonous behavior in the magnetic field, i.e. first increase and then decrease with the magnetic field strength eB and seem to saturate at $eB \gtrsim 2.5 \text{ GeV}^2$. In the small magnetic field, i.e.

⁴ Due to the parity in eB , the masses of their anti-particles should be the same.

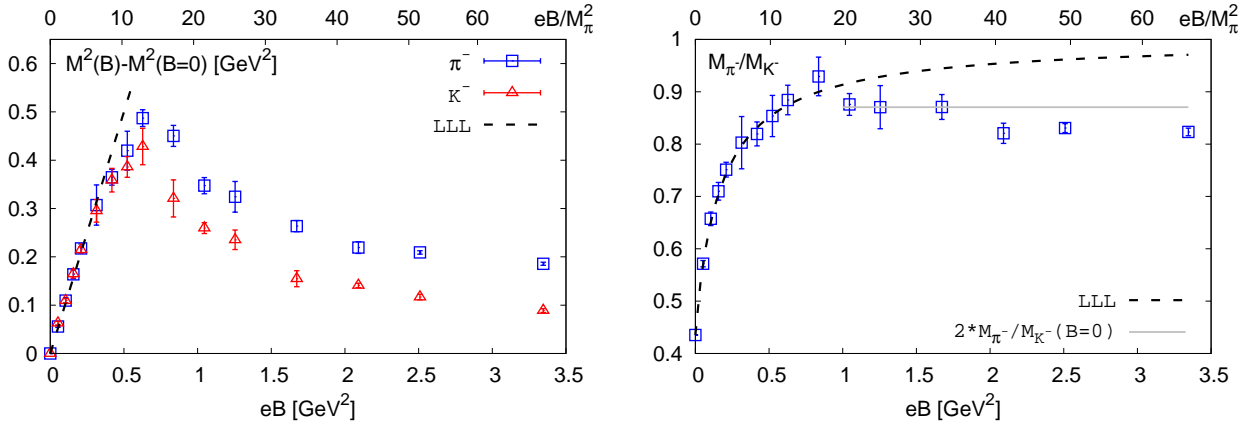


FIG. 6. Left: Differences of squared masses between the case at $B \neq 0$ and $B = 0$, $M^2(eB) - M^2(eB = 0)$ for π^- and K^- as a function of eB . Right: Ratio of the charged pion mass to charged kaon mass at nonzero magnetic field. Dashed lines in both plots show the results of the lowest Landau level approximation, while the grey horizontal line in the right plot gives the 2 times the value of M_{π^-}/M_{K^-} at $B = 0$.

$eB \lesssim 0.31 \text{ GeV}^2$ ($N_b \leq 6$), the differences, as labelled by blue circle and red triangle for π^- and K^- respectively, can be well described by the lowest Landau level (LLL) approximation (cf. Eq. 6) shown as the dashed line in the plot, while at larger eB , the masses start to deviate from the results of the LLL approximation and then decrease with eB . The deviation of M_{π^-} and M_{K^-} from the LLL approximation suggests that π^- and K^- cannot be considered as point-particles any more at $eB \gtrsim 0.31 \text{ GeV}^2$. The decreasing behavior of $M^2(B) - M^2(B = 0)$ in eB starts at a much weaker magnetic field, i.e. $eB \simeq 0.63 \text{ GeV}^2$ ($N_b=12$) compared to those obtained from quenched QCD [54], where a tendency of decreasing behavior sets in only till $eB \simeq 2 \text{ GeV}^2$. One can also observe that at large magnetic field the mass of K^- is less affected than π^- by eB , which is probably due to the fact that mass of K^- is larger than π^- in the vacuum as the case for neutral mesons. We further show the ratio $M_{K^-}(B)/M_{\pi^-}(B)$ in the right plot of Fig. 6. At vanishing magnetic field, the mass of π^- is about 40% of that of K^- , while as the magnetic field strength eB increases M_{π^-}/M_{K^-} firstly increases as reaching up to ~ 0.9 at $eB \sim 0.8 \text{ GeV}^2$, and then slightly decreases becoming flat at a value of ~ 0.8 at $eB \gtrsim 2 \text{ GeV}^2$. It is worth noting that this value is about 2 times the value of M_{π^-}/M_{K^-} at $B = 0$ as indicated by the grey horizontal line.

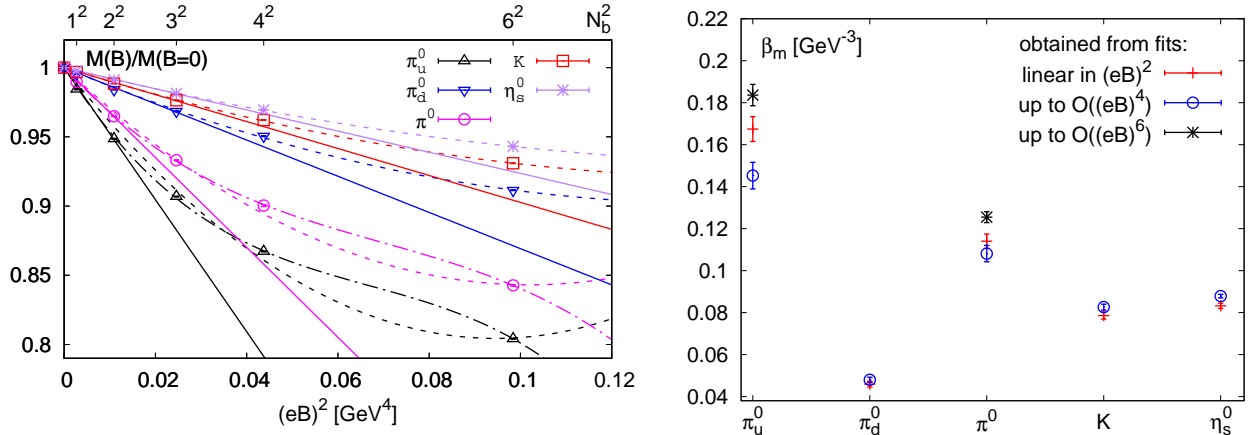


FIG. 7. Left: Ratio of masses of various neutral pseudo-scalar mesons to their values at zero magnetic field as a function of $(eB)^2$ in a small magnetic field region. The solid lines represent the fits to data points with an ansatz of $M(B)/M(B = 0) = 1 - 2\pi\beta_m (eB)^2/M(B = 0)$ with a fit range of $(eB)^2 \in [0, 0.03] \text{ GeV}^4$ except that for π_u^0 the fit range is $[0, 0.02] \text{ GeV}^4$, while dashed lines and the dash-dotted line denote fits with an ansatz of including higher order terms up to $(eB)^4$ and $(eB)^6$, respectively, with a fit range of $(eB)^2 \in [0, 0.1] \text{ GeV}^4$. Right: The obtained magnetic polarizability for the $u\bar{u}$ and $d\bar{d}$ flavor components of neutral pion, π^0 , neutral kaon and η_s^0 from the fits shown in the left plot. The fit results including fit ranges, fit ansatz and $\chi^2/d.o.f.$ are summarized in Table II.

As seen from Fig. 5 and Fig. 6 the neutral and charged pseudo-scalar mesons are not point-like particles any more in the strong magnetic field and their internal structures could be described by the magnetic dipole polarizability. In the relativistic case the energy squared of a pseudo-scalar meson has the following form [54]

$$M^2(B) = M^2(B=0) + |qB| - 4\pi M(B=0) \beta_m (eB)^2 - 4\pi M(B=0) \beta_m^{1h} (eB)^4 + \mathcal{O}((eB)^6), \quad (28)$$

where q is the electric charge of the particle, β_m is the magnetic dipole polarizability and β_m^{1h} is the first order magnetic hyper-polarizability. In the weak magnetic field we thus fit the ratio of neutral pseudo-scalar meson mass at nonzero magnetic field to its value at zero magnetic field using the following ansatz [54]

$$\frac{M(B)}{M(B=0)} = 1 - \frac{2\pi}{M(B=0)} \beta_m (eB)^2 - \frac{2\pi}{M(B=0)} \beta_m^{1h} (eB)^4 + \mathcal{O}((eB)^6). \quad (29)$$

We show $M(B)/M(B=0)$ for the case of neutral pseudo-scalar mesons in a small magnetic field range in the left plot of Fig. 7. A clear linear behavior in $(eB)^2$ can be observed for π_d^0 , K and η_s^0 at $(eB)^2 \lesssim 0.03 \text{ GeV}^2$ ($N_b \leq 3$) while for π_u^0 in a smaller window, i.e. at $(eB)^2 \lesssim 0.02 \text{ GeV}^2$ ($N_b \leq 2$). We thus fit the data in the corresponding range with the ansatz Eq. 29 including only the terms up to $(eB)^2$ and the fits are denoted by solid lines in the plot. The obtained magnetic dipole polarizabilities β_m are shown as red points in the right plot of Fig. 7. To check the uncertainties of β_m we also performed the fits to the data in a wider range of $(eB)^2 < 0.1 \text{ GeV}^2$ ($N_b \leq 6$) by adding higher order terms in the fit ansatz. It can be seen from the left plot of Fig. 7 that the fit ansatz including terms up to $(eB)^4$ (denoted as dashed lines) can describe the data for π_d^0 , K and η_s^0 fairly well, while an even higher order term, i.e. $(eB)^6$ is needed to describe the data for π_u^0 (denoted as a dashed-dotted line). The corresponding results of β_m from fits including terms up to $(eB)^4$ and $(eB)^6$ are shown as blue and black points in the right plot of Fig. 7, respectively. It can be seen that the uncertainties of β_m for π_d^0 , K and η_s^0 are mild while for π_u^0 are relatively large. β_m for the $d\bar{d}$ component of neutral pion is close to the half of that for η_s^0 and K , which could be due to different constituent quark masses and electric-magnetic interactions. In case of π_u^0 β_m is about 0.167 obtained from the linear fit in $(eB)^2$ and drops (increases) by about 15% (10%) obtained from fits including terms up to $(eB)^4$ ($(eB)^6$). The value of β_m for π_u^0 is thus in the ballpark of 4 times the value of β_m for π_d^0 , which is consistent with the qB scaling shown in the right plot of Fig. 5 due to $(q_u)^2 = 4(q_d)^2$. The qB scaling can also be seen from the values of the first order hyper-polarizabilities for π_u^0 and π_d^0 , i.e. $\beta_{m,\pi_u^0}^{1h} \simeq 16 \beta_{m,\pi_d^0}^{1h}$ as seen from Table II with the fit range $N_b \leq 6$. We also show the results of π^0 , which are obtained using the same fit policy as that for π_d^0 in Fig. 7 and Table II. The quality of the fit for π^0 is similar to that for π_d^0 , and the obtained β_m (β_m^{1h}) of π^0 from the best fit with smallest $\chi^2/d.o.f.$ is about 1.5 (5) times as those of both K and η_s^0 .

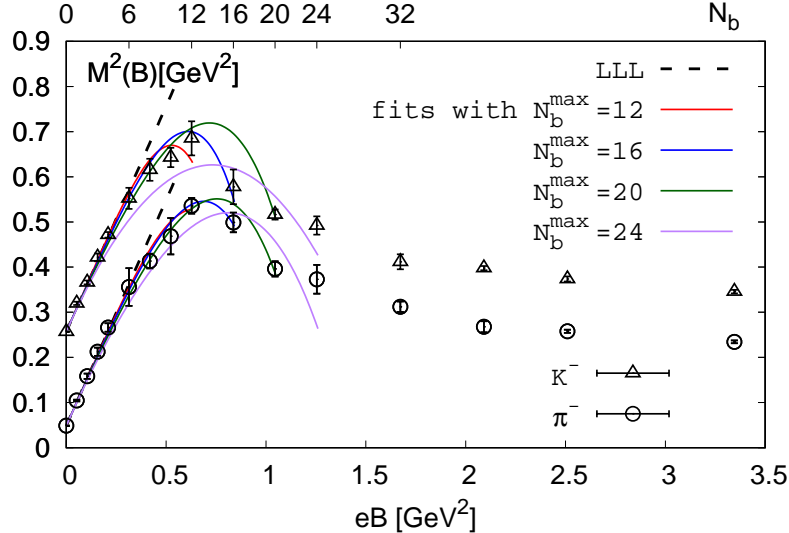


FIG. 8. Fits to the squared masses of charged pion and kaon using the ansatz Eq. 28 to extract magnetic dipole polarizability. Solid lines represent fit results with different fit ranges of $N_b^{max}=12, 16, 20$ and 24 while black dashed lines represent the results from the LLL approximation. The fit results including fit ranges, fit ansatz and $\chi^2/d.o.f.$ are summarized in Table II.

We move forward to show the results of magnetic polarizabilities for charged pseudo-scalar mesons, i.e. π^- and K^- based on a fit ansatz of Eq. 28 including terms up to $(eB)^4$. We performed fits to $M^2(B)$ using 4 different fit ranges,

i.e. $N_b \leq 12, 16, 20$ and 24 and the corresponding fit results are denoted by lines with $N_b^{max}=12, 16, 20$ and 24 in Fig. 8, respectively ⁵. The best fit is obtained with the narrowest fit range of $N_b^{max}=12$ whose $\chi^2/d.o.f.$ is closest to unity as listed in Table II. We find that the resulting β_m is consistent with zero for both π^- and K^- , while values of β_m^{1h} for π^- and K^- are comparable to be around 0.3 GeV^{-7} . As the fit range becomes wider the quality of the fit becomes worse, and this indicates that higher order hyper-polarizabilities are needed to describe the data which is beyond the scope of the current paper.

channel	$\beta_m [\text{GeV}^{-3}]$	$\beta_m^{1h} [\text{GeV}^{-7}]$	$\chi^2/d.o.f.$	fit ansatz & range
π_u^0	0.167(6)	-	31.3	up to $\mathcal{O}((eB)^2)$, $N_b \in [0, 2]$
	0.145(6)	-0.77(7)	410.3	up to $\mathcal{O}((eB)^4)$, $N_b \in [0, 6]$
	0.184(5)	-2.3(2)	25.1	up to $\mathcal{O}((eB)^6)$, $N_b \in [0, 6]$
π_d^0	0.046(1)	-	10.9	up to $\mathcal{O}((eB)^2)$, $N_b \in [0, 3]$
	0.048(1)	-0.17(1)	11.0	up to $\mathcal{O}((eB)^4)$, $N_b \in [0, 6]$
π^0	0.114(3)	-	9.3	up to $\mathcal{O}((eB)^2)$, $N_b \in [0, 2]$
	0.108(4)	-0.53(4)	49.7	up to $\mathcal{O}((eB)^4)$, $N_b \in [0, 6]$
	0.125(3)	-1.3(1)	3.5	up to $\mathcal{O}((eB)^6)$, $N_b \in [0, 6]$
K	0.079(2)	-	7.8	up to $\mathcal{O}((eB)^2)$, $N_b \in [0, 3]$
	0.083(1)	-0.26(2)	6.8	up to $\mathcal{O}((eB)^4)$, $N_b \in [0, 6]$
η_s^0	0.083(1)	-	9.5	up to $\mathcal{O}((eB)^2)$, $N_b \in [0, 3]$
	0.0878(8)	-0.252(9)	5.8	up to $\mathcal{O}((eB)^4)$, $N_b \in [0, 6]$
π^-	-0.00(5)	0.4(1)	1.3	up to $\mathcal{O}((eB)^4)$, $N_b \in [0, 12]$
	0.03(3)	0.25(5)	1.3	-, $N_b \in [0, 16]$
	0.08(2)	0.14(2)	1.9	-, $N_b \in [0, 20]$
	0.15(3)	0.06(3)	5.6	-, $N_b \in [0, 24]$
K^-	-0.02(2)	0.30(9)	1.9	up to $\mathcal{O}((eB)^4)$, $N_b \in [0, 12]$
	0.01(2)	0.16(4)	2.4	-, $N_b \in [0, 16]$
	0.05(2)	0.06(2)	4.2	-, $N_b \in [0, 20]$
	0.11(2)	0.00(2)	10.0	-, $N_b \in [0, 24]$

TABLE II. The magnetic dipole polarizability β_m and the first order hyper-polarizability β_m^{1h} of neutral mesons $\pi_u^0, \pi_d^0, \pi^0, K$ and η_s^0 as well as charged mesons π^- and K^- , fit ranges and fit ansatz as well as $\chi^2/d.o.f.$ obtained from fits shown in Figs. 7 and 8.

We close this subsection by comparing our results of magnetic polarizabilities (cf. Figs. 7 and 8 and Table II) to previous computations of β_m for light pseudo-scalar mesons in lattice QCD which were all done in the quenched approximation [52–54, 78]. In these quenched QCD studies the corresponding pion mass from the tuned valence quark mass at zero magnetic field is generally large, e.g. $M_\pi(eB=0) \gtrsim 512 \text{ MeV}$ in [78], $M_\pi(eB=0) \gtrsim 320 \text{ MeV}$ in [53, 54] and $M_\pi(eB=0) \gtrsim 400 \text{ MeV}$ in [52]. One difference to be noted is that in Ref. [52] β_m for π_u is about twice of that for π_d , while in our case β_m is about four times as that for π_d as consistent with the $|qB|$ scaling. This could be due to the fact that sufficiently small magnetic field needs to be used to extract β_m and relatively larger weakest magnetic fields are applied in [52]. As pointed in Ref. [52] the hopping parameter κ used in the Wilson propagator needs to be along the line of constant physics in the magnetic field, i.e. κ is eB dependent, β_m obtained from [78] with κ as a constant in eB might become smaller when the eB dependence of κ was taken into account as indicated from study in [52]. On the other hand, studies performed using Overlap valence quarks in quenched QCD on 18^4 and 20^4 lattices give a nonzero value of β_m for charged pion which are close to the experiment results obtained from the COMPASS collaboration, i.e. $\beta_m = (-2.0 \pm 0.6_{stat} \pm 0.7_{syst}) \times 10^{-4} \text{ fm}^3$ [79]. Note that the experiment value of β_m is obtained under the assumption that electrical polarizability $\alpha_\pi = -\beta_m$ [79]. While in our study the value of β_m for charged pion is consistent with zero, thus aiming for a comparison to experiment results of magnetic polarizability a study with continuum extrapolations at physical pion mass is crucially needed.

⁵ The reason we choose the smallest value of N_b^{max} to be 12 is that at $N_b \leq 6$ the data can be well described by the LLL approximation and at least 3 more data points are needed to accommodate a 2-parameter fit.

B. Light quark chiral condensates

As has been pointed out in Ref. [9] the presence of the external magnetic field does not introduce any new eB -dependent divergences. To take care of the additive divergences as well as the multiplicative renormalization in the chiral condensate, we investigate the following dimensionless quantity [10],

$$\Sigma_l(B) = \frac{2m_l}{M_\pi^2 f_\pi^2} (\langle \bar{\psi}\psi \rangle_l(B \neq 0) - \langle \bar{\psi}\psi \rangle_l(B = 0)) + 1, \quad (30)$$

where $m_l \equiv m_u \equiv m_d$ is the bare quark mass for up and down quarks, and M_π and f_π is the mass of pion and pion decay constant respectively at zero magnetic field. In our study M_π is found to be 220.61(6) MeV while f_π is 96.93(2) MeV whose determination will be shown in Section IV C.

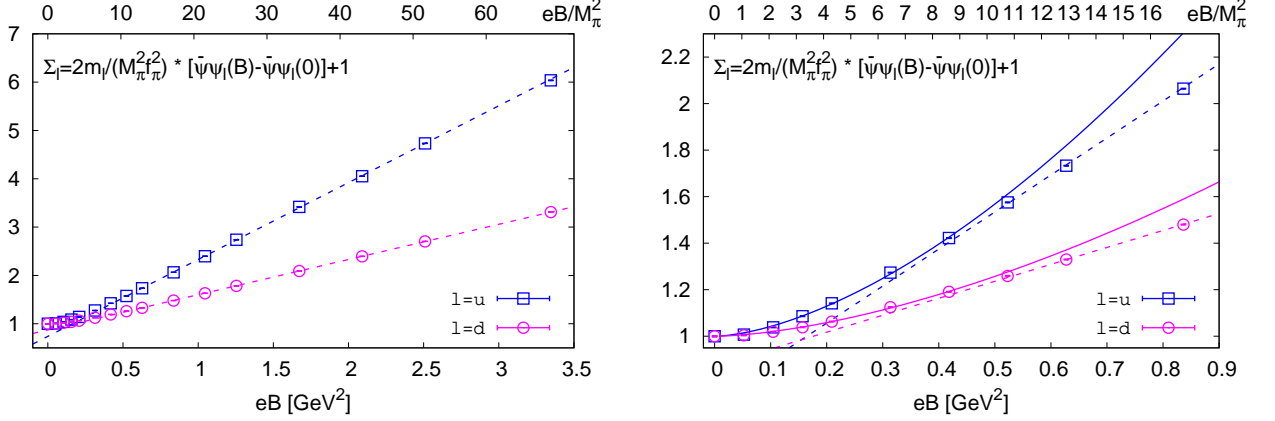


FIG. 9. Left: Renormalized up and down quark chiral condensates as a function of magnetic field strength eB . The left plot shows chiral condensates in the whole eB region while the right one shows those in a narrower eB region. The dashed lines in both plots denote two-parameter linear fits of chiral condensates at $eB \geq 0.5 \text{ GeV}^2$ while the solid lines in the right plot represent power-law fits with ansatz of $h(eB)^\gamma + 1$ at $eB \leq 0.5 \text{ GeV}^2$.

We show Σ_u and Σ_d as a function of eB in Fig. 9. As expected that due to different electric charges of up and down quarks up quark and down quark chiral condensates becomes non-degenerate in the nonzero magnetic field. And the up quark chiral condensate is more affected compared to that of the down quark one by the magnetic field which is probably due to $|q_u| > |q_d|$. It is obvious to see that at large magnetic field both up and down quark chiral condensates show linear behavior in eB . We perform linear fits for these two condensates at $(eB) \gtrsim 0.5 \text{ GeV}^2$, and the corresponding fit results, which are shown as dashed lines in Fig. 9, describe the data fairly well. We find that the

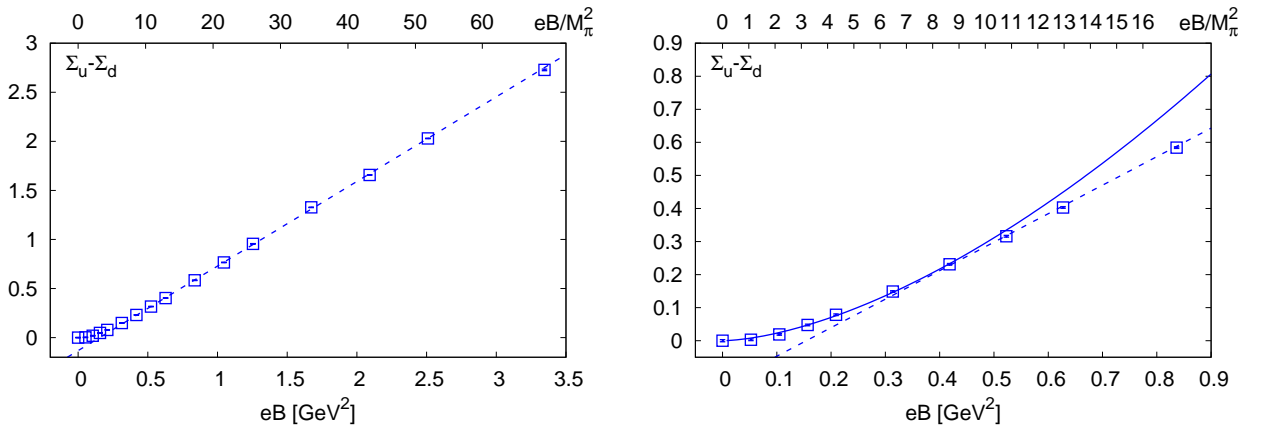


FIG. 10. Similar as Fig. 9 but for the difference of renormalized quark chiral condensates $\Sigma_u - \Sigma_d$. The solid line represent a two-parameter power-law fit with an ansatz of $h|eB|^\gamma$ while the dashed lines denote two-parameter linear fits in eB .

slope for the up quark condensate obtained from the linear fit is 1.591(5) and it is about twice as that for the down quark which is 0.729(1). While the linear fit works for strong magnetic fields, it is not the case any more at $eB \lesssim 0.5 \text{ GeV}^2$ as seen from a blowup plot of the left plot of Fig. 9, i.e. the right plot of Fig. 9. At $eB \lesssim 0.5 \text{ GeV}^2$ both chiral condensates increase faster than a linear behavior in eB . We thus adopt a two-parameter power-law fit ansatz of $h|eB|^\gamma + 1$ to fit the chiral condensates. We found that this fit ansatz can describe the data at $eB \lesssim 0.5 \text{ GeV}^2$ well and the exponent γ obtained for these two condensates are almost the same, i.e. $\gamma = 1.62(4)$ for the up quark chiral condensate while $\gamma = 1.61(4)$ for the down quark chiral condensate. We also show the difference of up and down quark chiral condensates $\Sigma_u - \Sigma_d$ in Fig. 10. Similar as the fits we showed in Fig. 9 we performed two-parameter linear fits (shown as the dashed line) at $eB \gtrsim 0.5 \text{ GeV}^2$ and two-parameter power-law fits (shown as the solid line) at $eB \lesssim 0.5 \text{ GeV}^2$. It is expected that $\Sigma_u - \Sigma_d$ posses a linear behavior in large eB , and a power-law behavior with the same exponent as that in Fig. 9 at $eB \lesssim 0.5 \text{ GeV}^2$.

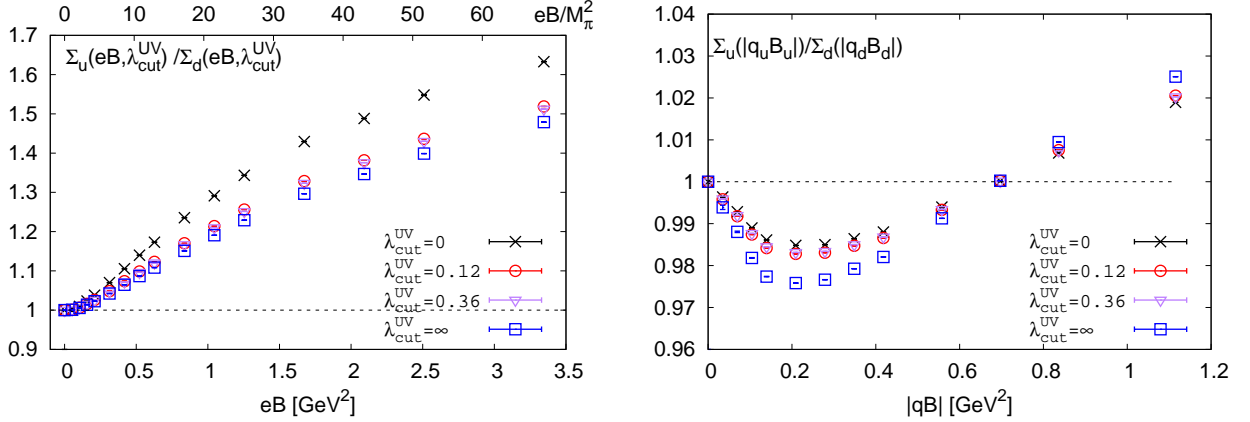


FIG. 11. Left: Ratio of renormalized up quark condensate to the down quark one $\Sigma_u(eB)/\Sigma_d(eB)$ as a function of eB . Right: Similar as the left plot but as a function of $|qB| = |q_u B_u| = |q_d B_d|$. In both plots $\lambda_{cut}^{UV} = 0$ corresponds to the case that the subtrahend in the renormalized chiral condensate is $\langle \bar{\psi}\psi \rangle_l(B=0)$ (c.f. Eq. 30), and $\lambda_{cut}^{UV} = \infty$ to the unsubtracted chiral condensate, i.e. the subtrahend is 0, and $\lambda_{cut}^{UV} = 0.12$ and 0.36 gives the uncertainty on the estimate of UV divergence part of the chiral condensates as the subtrahend in Eq. 31.

We further show the ratio of Σ_u/Σ_d in Fig. 11. To better understand the influence of the UV divergence part of the chiral condensate in the ratio we also investigate the following quantity,

$$\Sigma_l(B, \lambda_{cut}^{UV}) = \frac{2m_l}{M_\pi^2 F_\pi^2} (\langle \bar{\psi}\psi \rangle_l(B) - \langle \bar{\psi}\psi \rangle_l^{UV}(B=0, \lambda_{cut}^{UV})) + 1, \quad (31)$$

where λ_{cut}^{UV} is the lower limit of λ in the integration in Eq. 27 which gives the UV divergence part of the chiral condensate, i.e. $\langle \bar{\psi}\psi \rangle_l^{UV}(B=0, \lambda_{cut}^{UV})$. It is obvious that when $\lambda_{cut}^{UV} = 0$ Eq. 31 is the same as Eq. 30, i.e. $\Sigma_l(B, \lambda_{cut}^{UV} = 0) \equiv \Sigma_l(B)$, and when $\lambda_{cut}^{UV} = \infty$ $\langle \bar{\psi}\psi \rangle_l^{UV}(B=0, \lambda_{cut}^{UV} = \infty)$ goes to zero and the left hand side of Eq. 31 $\Sigma_l(B, \lambda_{cut}^{UV} = \infty)$ equals to $\frac{2m_l}{M_\pi^2 F_\pi^2} \langle \bar{\psi}\psi \rangle_l(B) + 1$. We see in the left plot of Fig. 11 that the ratio Σ_u/Σ_d obtained using different values of λ_{cut}^{UV} all increases with increasing strength of the magnetic field eB , which is a consequence that $\Sigma_u - \Sigma_d$ increases faster in eB than Σ_d . Results obtained using $\lambda_{cut}^{UV} = 0$ and ∞ show two extreme cases that Σ_l is obtained by subtracting the full chiral condensate at zero magnetic field $\langle \bar{\psi}\psi \rangle_l(B=0)$, and by subtracting zero, respectively. The obtained ratio $\Sigma_u(eB)/\Sigma_d(eB)$ in these two extreme cases as shown in the left plot of Fig. 11 differs at most about 10%. To avoid the subtraction of the infrared contribution to $\langle \bar{\psi}\psi \rangle_l$, we estimated the UV-divergence contribution to $\langle \bar{\psi}\psi \rangle_l$ with $\lambda_{cut}^{UV} \in [0.12, 0.36]$ as discussed in Section III D. As shown in the plot the obtained $\Sigma_u(eB)/\Sigma_d(eB)$ lies in between the two extreme cases and the difference between results obtained using $\lambda_{cut}^{UV} = 0.12$ and 0.36 is mild.

Keeping in mind the fact of qB scaling for the u and d flavor components of the neutral pion mass, we also show the ratio of Σ_u and Σ_d at same values of $|qB| = |q_u B_u| = |q_d B_d|$ in the right plot of Fig. 11. Results obtained using various values of λ_{cut}^{UV} are also shown. We find that the ratio $\Sigma_u(|q_u B_u|)/\Sigma_d(|q_d B_d|)$ is very close to unity with deviation at most by 3% with qB up to about 1.1 GeV². We thus conclude that the qB scaling of light quark chiral condensates holds within an accuracy of 3% in our current window of magnetic field.

To compare with the results from χ PT we then show the average of chiral condensates, i.e. $\Sigma_{avg} = (\Sigma_u + \Sigma_d)/2$ in Fig. 12 together with the results from χ PT. Although our results are not yet continuum extrapolated and are obtained at a single lattice cut-off with lattice spacing $a \simeq 0.117 \text{ fm}$, as compared with results from Ref. [10] where the finest

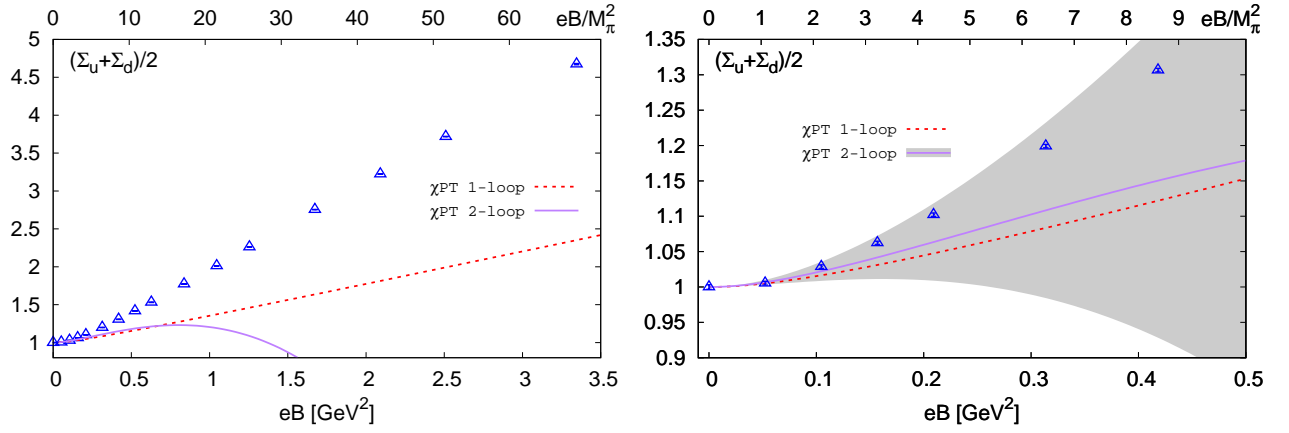


FIG. 12. Left: Average of the up and down quark chiral condensates as a function of magnetic field strength eB . Right: Same as the left plot but a blow up in the small values of eB . The red dashed line stands for the one-loop χ PT results [16, 80] while the purple solid line with a grey band represents the two loop χ PT results [81].

lattice spacing is 0.1 fm our results should be close to the results in the continuum limits besides that we are using a Highly Improved Staggered fermions which has a smaller taste system breaking effects [66]. By comparing to the one loop χ PT results extended to nonzero pion mass (dashed lines in the plot) we find that the results from χ PT describe our lattice data only at the weakest magnetic field of $eB = 0.052 \text{ GeV}^2$, which is already at the scale of $M_\pi^2(eB = 0)$. While the two-loop χ PT results are slightly larger than those from the one-loop, it has large uncertainties (denoted as the grey band) arising from the undetermined low energy constants. It is worth noting that our pion mass at $eB = 0$ is heavier than the physical one, and both one-loop and two-loop chiral perturbation theory give slightly smaller results for $(\Sigma_u + \Sigma_d)/2$ with larger pion mass.

C. Decay constants of neutral pion and kaon and the GMOR relation

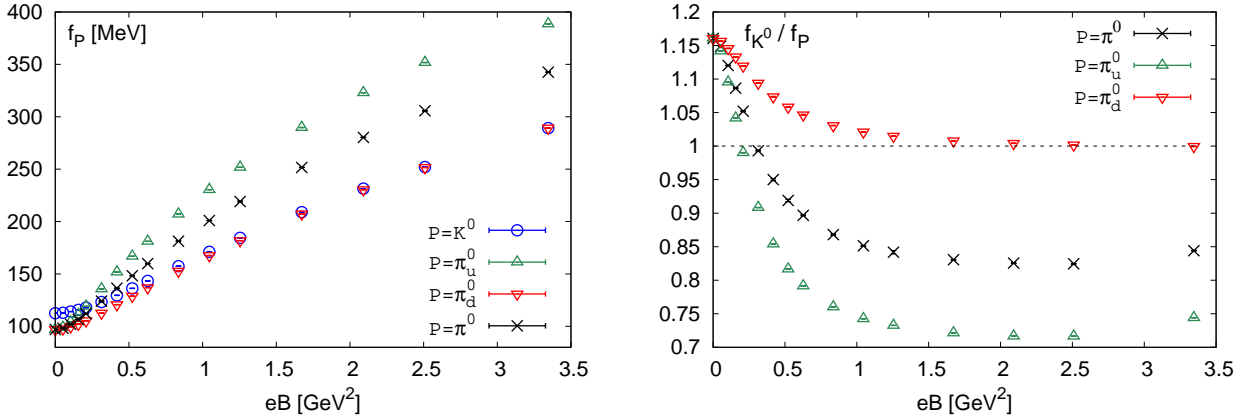


FIG. 13. Left: eB dependence of decay constants of π_u^0 , π_d^0 , π^0 and K^0 . Right: Ratio of neutral kaon decay constant to other three decay constants as a function of eB .

We start by showing decay constants of neutral pion and kaon in Fig. 13. At $eB = 0$ we obtained pion decay constant $f_\pi = 96.93(2) \text{ MeV}$ and kaon decay constant $f_K = 112.50(2) \text{ MeV}$ resulting $f_K/f_\pi = 1.1606(3)$. The errors quoting here are purely statistical ones. These three results are rather close to those obtained at the physical mass point in the continuum limit as quoted in the latest FLAG review, i.e. $f_\pi = 92.1(6) \text{ MeV}$, $f_K = 110.1(5) \text{ MeV}$ and

$f_K/f_\pi=1.1917(37)$ [82]⁶. As seen from the left plot of Fig. 13 all the decay constants increase with eB , where the decay constants from the up quark flavor component of neutral pion, $f_{\pi_u^0}$ increases most rapidly with respect to eB while f_{K^0} is the least. It is interesting to see that f_{K^0} becomes degenerate with the decay constant of the down quark flavor component of neutral pion $f_{\pi_d^0}$ in the large magnetic field. The value of neutral pion decay constant f_{π^0} , as extracted from an average on the correlation function of $G_{\pi_u^0}$ and $G_{\pi_d^0}$ in the same way as we did for M_{π^0} in Section IV A, lies in between the results of $f_{\pi_u^0}$ and $f_{\pi_d^0}$. We also show the ratio of f_{K^0} to other three decay constants in the right plot of Fig. 13. It is interesting to see that the ratio $f_{K^0}/f_{\pi_d^0}$ firstly decreases with increasing eB and saturates to be unity at $eB \gtrsim 1.5\text{GeV}^2$, while both $f_{K^0}/f_{\pi_u^0}$ and f_{K^0}/f_{π^0} decreases faster in eB as compared to $f_{K^0}/f_{\pi_d^0}$, and goes below unity at $eB \gtrsim 0.2\text{GeV}^2$. In the large magnetic field $f_{K^0}/f_{\pi_u^0}$ and f_{K^0}/f_{π^0} seems to saturate to be ~ 0.7 and ~ 0.85 , respectively, in the range of $eB \in (1.5, 2.5)\text{GeV}^2$, and then slightly increase by less than 5% at our largest value of eB .

As seen from Fig. 5 and Fig. 11 there exists qB scaling behavior in $M_{\pi_u^0}(M_{\pi_d^0})$ and $\Sigma_u(\Sigma_d)$ we also wonder about the case for the up and down quark flavor components of neutral pion decay constant. We show the ratio $f_{\pi_u^0}(|q_u B_u|)/f_{\pi_d^0}(|q_d B_d|)$ as a function of $|qB|$ in the left plot of Fig. 14. It can be clearly seen that the ratio is very close to 1 and the deviation is always less than 2% in our current window of magnetic field studied. Thus the qB scaling behavior is also found in the case of neutral pion decay constant. As $M_{\pi_u^0}(M_{\pi_d^0})$, $\Sigma_u(\Sigma_d)$ and $f_{\pi_u^0}(f_{\pi_d^0})$ are all related to the pion correlation functions, i.e. $G_{\pi_u^0}(\tau)$ and $G_{\pi_d^0}(\tau)$, we show the ratio of $G_{\pi_u^0}(\tau, q_u B_u)/G_{\pi_d^0}(\tau, q_d B_d)$ as a function of temporal distance n_τ at 13 different values of $|qB|$ in the right plot of Fig. 14. We found that at large distance, i.e. n_τ close to 48 ($N_\tau/2$) which is most relevant to the quantities we discussed earlier, the ratio deviates from unity at most by 2%. This naturally explains the consistency of the qB scaling behavior shown in $M_{\pi_u^0}(M_{\pi_d^0})$, $\Sigma_u(\Sigma_d)$ and $f_{\pi_u^0}(f_{\pi_d^0})$.

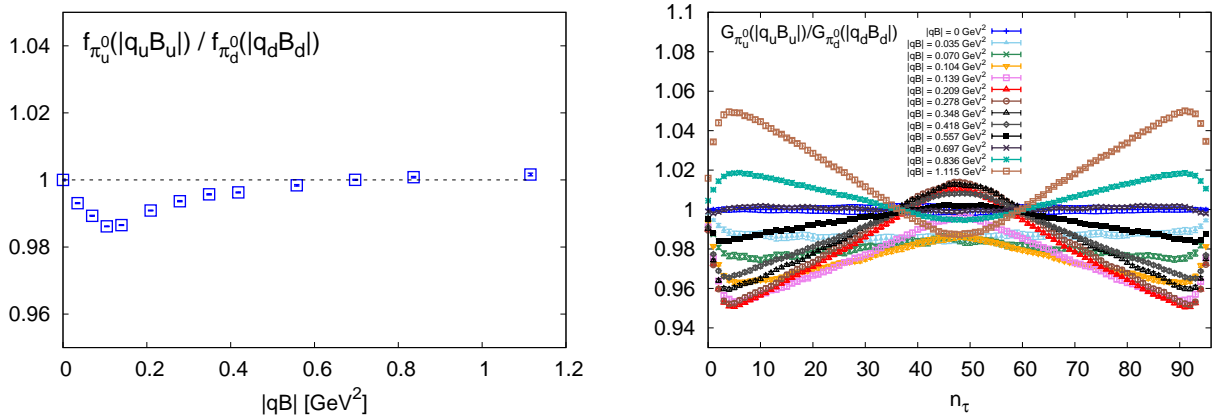


FIG. 14. Left: Ratio of $f_{\pi_u^0}$ to $f_{\pi_d^0}$ at same value of $|qB| = |q_u B_u| = |q_d B_d|$ as a function of $|qB|$. Right: $G_{\pi_u^0}(n_\tau, |q_u B_u|)/G_{\pi_d^0}(n_\tau, |q_d B_d|)$ as a function of temporal distance n_τ at various values of $|qB| = |q_u B_u| = |q_d B_d|$.

Since we have obtained the masses and decay constants of neutral pseudo-scalar mesons, light and strange quark chiral condensates, we are now ready to check the validity of the 2-flavor as well as the 3-flavor GMOR relations. We show the corrections to the 2-flavor and 3-flavor GMOR relations in a wide window of eB from 0 to $\sim 3.35\text{GeV}^2$ in the left and right plots of Fig. 15, respectively. In the left plot of Fig. 15 the next-to-leading order chiral correction $\delta_{\pi_{u,d}^0}$ (cf. Eq. 14 and Eq. 15) for u and d quark flavor components separately. To get a UV-free chiral condensate, as discussed in Section III D, we subtract the UV-divergence part $\langle \bar{\psi}\psi \rangle_l^{UV}$ obtained using $\lambda_{cut}^{UV} = 0.12$ and 0.36 from the chiral condensates $\langle \bar{\psi}\psi \rangle_l$. The results obtained using $\lambda_{cut}^{UV} = 0.12$ and 0.36 are shown as open and filled points, respectively. At zero magnetic field the correction to the GMOR relation at most is about 6%. As the GMOR relation strictly holds in the chiral limit of quarks at zero magnetic field from the leading order chiral perturbation theory, the next to leading order chiral corrections to the 2-flavor GMOR relation at the physical pion mass M_π is $(6.2 \pm 1.6)\%$ [33, 34]. Although in our study the pion mass at $eB = 0$ is 220 MeV, the corrections to the GMOR relation at

⁶ Note that there is a factor of $\sqrt{2}$ difference in convention for the decay constant in our paper and Ref. [82]. The numbers shown here from Ref. [82] are already divided by $\sqrt{2}$ for comparison to our results.

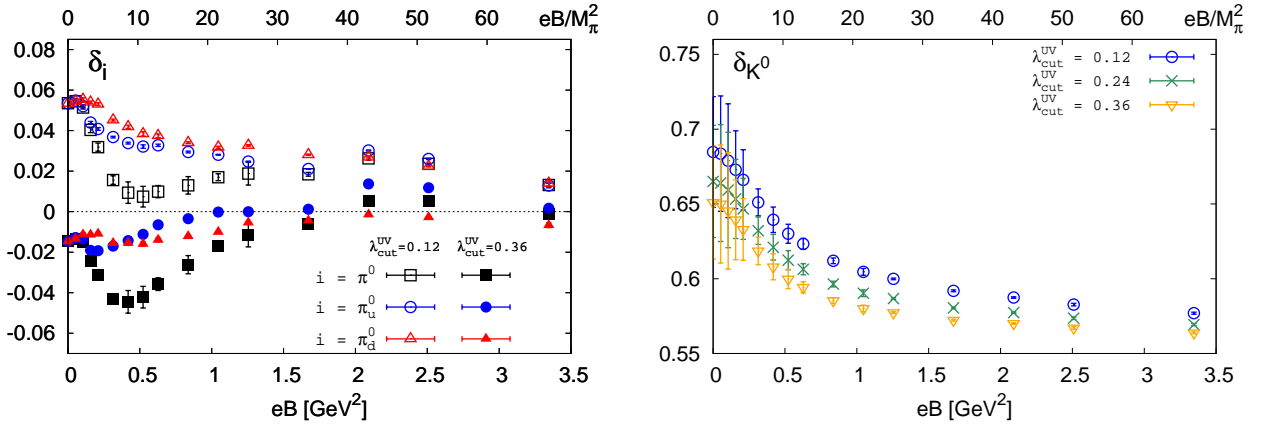


FIG. 15. The next-to-leading order chiral corrections $\delta_{i=\pi^0, \pi_u^0, \pi_d^0}$ for the 2-flavor GMOR relation (left) and δ_{K^0} for the 3-flavor GMOR relation (right).

$eB=0$ shown in Fig. 15 is in the same ballpark. At nonzero magnetic field we see that the correction either decreases or increases towards unity and compared to the case at $eB = 0$ $|\delta_{\pi_{u,d}^0}|$ becomes smaller at $eB \gtrsim 1.5$ GeV². This is to say that the deviation of $\delta_{\pi_{u,d}^0}$ from zero is at most 6% in the whole range of magnetic field strength studied. We thus conclude that in our study the GMOR relation for the up and down quark flavor components of π^0 holds with an accuracy of $\sim 6\%$ in $eB \in [0, 3.35]$ GeV². While for π^0 the correction δ_{π^0} is obtained by averaging up and down quark flavor components of the correlation function with the disconnected part of the correlation function being ignored in our study. We also see that the GMOR relation for neutral pion π^0 (cf. Eq. 7) holds quite well in the range of eB from 0 to 3.35 GeV².

We then have a look at the next-to-leading order chiral correction δ_{K^0} to the 3-flavor GMOR relation (cf. Eq. 8) shown in the right plot of Fig. 15. The UV-divergence of the strange quark chiral condensate is taken care of in the same way as for the light quark chiral condensate. At zero magnetic field the chiral correction δ_K is much larger than δ_π due to an enhancement factor M_K^2/M_π^2 [32]. At $eB = 0$ δ_K is roughly in the range of (60-72)% from our computation while chiral perturbation theory combined with the QCD sum rules give $\delta_K = (55 \pm 5)\%$ [35] at the physical mass point. As eB increases δ_K decreases and seems to saturate at about 56% at $eB \gtrsim 2.5$ GeV². Thus in the nonzero magnetic field the correction to the 3-flavor GMOR relation becomes smaller, and it is reduced by about 15% at our largest value of eB compared to the case at $eB = 0$.

V. CONCLUSIONS

In this paper we investigated the masses and magnetic polarizabilities of light and strange pseudo-scalar mesons, chiral condensates, as well as neutral pion and kaon decay constants in the presence of background magnetic fields with $eB \lesssim 3.35$ GeV² by performing lattice simulations of $N_f = 2 + 1$ QCD at zero temperature using HISQ fermions with $m_\pi \approx 220$ MeV on $32^3 \times 96$ lattices at a single lattice cutoff $a = 0.117$ fm. Our main results include the qB scaling of various chiral observables and the eB -dependence of the corrections to 2- and 3-flavor GMOR relations. We find that the qB scaling of $M_{\pi_u^0}$ ($M_{\pi_d^0}$), Σ_u (Σ_d) and $f_{\pi_u^0}$ ($f_{\pi_d^0}$) as well as $G_{\pi_u^0}(\tau)$ ($G_{\pi_d^0}(\tau)$) in the range of $eB \in [0.05, 3.35]$ GeV². With complete Dirac eigenvalue spectrum we are able to estimate the UV-divergence of the quark chiral condensate. This render us to study the 2-flavor and 3-flavor GMOR relations. We found that the chiral corrections to the 2-flavor and 3-flavor GMOR relations are about 6% and 65% at $eB = 0$ in our setup, respectively. The correction to the 2-flavor GMOR relation for the neutral pion is less than 6% in the whole window of magnetic field we studied and becomes less than 2% at our strongest magnetic field. Thus the 2-flavor GMOR relation holds true with an accuracy of 6% at $eB \in [0, 3.35]$ GeV². This makes the connection of the reduction of T_{pc} and reduction of neutral pion mass in the nonzero magnetic field more clear. On a different note that the in the case of vanishing magnetic field the both sides of the GMOR relation has similar behavior in terms of breaking fields, e.g. quark mass at $eB = 0$. I.e. all the chiral observables, i.e. chiral condensates, pion decay constants as well as the pion mass decreases with lighter quark mass. However, this is not the case at nonzero magnetic fields, as the chiral condensate and neutral pion decay constants increase with larger eB , while the neutral pion mass decreases with larger eB as restricted by the 2-flavor GMOR relation. While for the second lightest Goldstone boson, i.e. neutral kaon in the magnetic field the correction

to the 3-flavor GMOR relation decreases monotonously as eB grows and saturates at $\sim 56\%$.

Concerning the meson spectrum we found that for both charged and neutral pseudo-scalar mesons the mass spectrum of lighter mesons are more affected by the magnetic field. For the neutral pseudo-scalar mesons their masses monotonously decrease as the magnetic field strength grows and then saturate at nonzero values at eB up to ~ 3.35 GeV². The nonzeroness of (connected) neutral pion mass thus disfavors an occurrence of a superconducting phase in the current window of magnetic field. For the charged pion and kaon, their masses show a non-monotonous behavior in eB , i.e. they firstly increase in eB following the behavior of the LLL approximation, and then increase slower than the LLL approximation and finally show a turning point with subsequent decreasing behavior in eB . The decreasing behavior of the charged pion mass is different from previous computations and this may be due to the fact that the magnetic field in terms of $M_\pi(eB=0)$ is much larger compared to previous cases. While the neutral pion cannot be considered as a point-like particle already at our smallest value of $eB \sim 0.05$ GeV² $\sim M_\pi^2(B=0)$, the charged pion remains point-like till eB at about $6M_\pi^2(B=0)$. The obtained magnetic polarizabilities of charged and neutral pions from the eB dependence of their masses are at odd with the results from quenched QCD as well as the experiment measurements where the magnetic polarizability is assumed to be the additive inverse of the electric polarizability. This and together with the different behavior of M_{π^-} at large eB leaves a plenty big room for studies in the future on the possible effects from dynamic quarks as well as discretization effects on the lattice in the weak and strong magnetic fields.

On the other hand the pion and kaon decay constants and their ratio are obtained as $f_\pi = 96.93(2)$ MeV, $f_K = 112.50(2)$ MeV and $f_K/f_\pi = 1.1606(3)$ at $eB = 0$ in our study. These results deviate by 5% from the state-of-the-art lattice QCD results obtained at the physical mass point and in the continuum limit. As eB increases both the neutral and kaon decay constants increase and the ratios between f_{K^0} and other three decay constants (f_{π^0} , $f_{\pi_u^0}$, $f_{\pi_d^0}$) monotonously decrease and then saturate at nonzero values at large eB . Since we only deal with the decay constants of neutral pseudo-scalar mesons that are related to the axial vector current which is parallel to the magnetic field at zero momentum, it would be interesting to study the new decay constants at nonzero momentum and those related to the vector current as well in the future.

ACKNOWLEDGEMENTS

We thank Swagato Mukherjee for the early involvement of the work and enlightening discussions, and thank Gunnar Bali, Toru Kojo, Jinfeng Liao, Zhaofeng Liu and Pengfei Zhuang for interesting discussions. This work was supported by the National Natural Science Foundation of China under grant numbers 11535012, 11775096 and 11947237, and the RIKEN Special Postdoctoral Researcher program. The numerical simulations have been performed on the GPU cluster in the Nuclear Science Computing Center at Central China Normal University (NSC³), Wuhan, China.

Appendix A: Generalized Ward-Takahashi identities in a background magnetic field

The general Ward-Takahashi identity in the continuum QCD in the nonzero magnetic field has already been derived, see e.g. Ref. [52]. Here In this appendix we will further derive the non-anomalous Ward-Takahashi identity related to the pseudo-scalar operator and vector operator correlation functions with chiral transformation in the presence of a magnetic field interacting with two degenerate light quark flavors. The main results are shown in Eqs. A.31, A.32, A.33 and A.37, where the first three identities are discussed in Fig. 3 in Section III C.

We start by showing the Ward-Takahashi identity at zero magnetic field with our conventions. The expectation value of an observable O in QCD is given by,

$$\langle O \rangle = \frac{1}{Z} \int \mathcal{D}G_\mu \mathcal{D}\bar{\psi} \mathcal{D}\psi e^{-S_{\text{QCD}}} O, \quad (\text{A.1})$$

where $O = O(y_1, \dots, y_n)$ is an position depending operator, $\langle 1 \rangle = 1$ and S_{QCD} is the Euclidean action,

$$S_{\text{QCD}} = \int d^4x \left(\frac{1}{2} \text{tr} G_{\mu\nu} G_{\mu\nu} + \bar{\psi} (\not{D} + M) \psi \right), \quad (\text{A.2})$$

and $G_{\mu\nu} = \partial_\mu G_\nu - \partial_\nu G_\mu - ig[G_\mu, G_\nu]$ and G_μ represents the gluon field. $M = \text{diag}(m_u, m_d, \dots)$ is a mass matrix. $\psi = (u, d, \dots)^\top$ is a flavor multiplet of quarks, spinor and color indexes are suppressed. $D_\mu = \partial_\mu - igG_\mu$ is the covariant derivative at the zero magnetic field.

The Ward-Takahashi identity [83, 84] for a local transformation

$$\begin{cases} \bar{\psi}(x) \rightarrow \bar{\psi}'(x) = \bar{\psi}(x) + \alpha(x)\bar{\psi}(x), \\ \psi(x) \rightarrow \psi'(x) = \psi(x) + \alpha(x)\psi(x). \end{cases} \quad (\text{A.3})$$

is written as,

$$\left\langle O \frac{\delta \log \mathcal{J}}{\delta \alpha(x)} \right\rangle - \left\langle O \frac{\delta S_{\text{QCD}}}{\delta \alpha(x)} \right\rangle + \left\langle \frac{\delta O}{\delta \alpha(x)} \right\rangle = 0. \quad (\text{A.4})$$

Here J is the Jacobian of the transformation, which represents the anomaly. The original relation between renormalization factors in QED was derived in [83], and it was generalized as a non-perturbative relation from the symmetry argument [84]. We rely on the Leibniz rule with the covariant derivative,

$$D_\mu(\alpha(x)\phi(x)) = (D_\mu\alpha(x))\phi(x) + \alpha(x)D_\mu\phi(x) \quad (\text{A.5})$$

and associated integrations by parts. If $\alpha(x)$ is a neutral scalar function, the covariant derivative reduces into partial derivative, $D_\mu\alpha(x) = \partial_\mu\alpha(x)$.

In the case of nonzero magnetic field we use the Landau gauge for the magnetic field A_μ pointing along the z (x_3) direction in the infinite volume, $A_\mu(x) = (A_1, A_2, A_3, A_4) = (0, Bx_1, 0, 0)$. The covariant derivative with the magnetic field thus becomes

$$D_\mu \rightarrow \tilde{D}_\mu = \partial_\mu - igG_\mu - ieA_\mu Q^3, \quad (\text{A.6})$$

where

$$Q^3 = \frac{1}{6}\sigma^0 + \frac{1}{2}\sigma^3 = \frac{1}{6}\mathbf{1} + t^3, \quad (\text{A.7})$$

and σ^i is any of three Pauli matrices with $i = 1, 2, 3$ and the unit matrix with $\sigma^0 = \mathbf{1}$, and Q^3 has the following commutation relation with $t^i \equiv \sigma^i/2$,

$$Q^3 t^i = t^i Q^3 - iT_i^{12}, \quad (\text{A.8})$$

where $T_i^{12} = (\delta_{i2}t^1 - \delta_{i1}t^2)$.

1. Chiral rotation for the action

We show the derivation of $\frac{\delta S_{\text{QCD}}}{\delta \alpha^i(x)}$ in this subsection. Let us firstly introduce a scalar function $\alpha^i(x)$ which represents an infinitesimal local transformation. The local chiral rotation is then,

$$\begin{cases} \bar{\psi}(x) \rightarrow \bar{\psi}'(x) = \bar{\psi}(x) + \alpha^i(x)\bar{\psi}(x)t^i\gamma_5, \\ \psi(x) \rightarrow \psi'(x) = \psi(x) + \alpha^i(x)\psi(x)t^i\gamma_5. \end{cases} \quad (\text{A.9})$$

The kinetic term in the action is then transformed in the leading order of $\alpha^i(x)$ as,

$$\bar{\psi}\gamma_\mu D_\mu\psi \rightarrow \bar{\psi}(x)\gamma_\mu D_\mu\psi(x) + \bar{\psi}(x)\gamma_\mu D_\mu(\alpha^i(x)t^i\gamma_5\psi(x)) + \alpha^i(x)\bar{\psi}(x)t^i\gamma_5\gamma_\mu D_\mu\psi(x). \quad (\text{A.10})$$

The second term in the right hand side of the arrow sign in Eq. A.10 can be decomposed by the Leibniz rule,

$$\bar{\psi}(x)\gamma_\mu D_\mu(\alpha^i(x)t^i\gamma_5\psi(x)) = \bar{\psi}(x)\gamma_\mu(\partial_\mu\alpha^i(x))t^i\gamma_5\psi(x) + \bar{\psi}(x)\alpha^i(x)\gamma_\mu D_\mu(t^i\gamma_5\psi(x)). \quad (\text{A.11})$$

In the hereafter derivation we assume a flavor symmetry $M = m\mathbf{1}$, the mass term then transforms as,

$$\bar{\psi}(x)\psi(x) \rightarrow \bar{\psi}(x)\psi(x) + 2\alpha^i(x)\bar{\psi}(x)t^i\gamma_5\psi(x). \quad (\text{A.12})$$

We now derive the variation of the QCD action under the chiral transformation when $eB = 0$ and $eB \neq 0$ as follows

a. Zero magnetic field For the case of vanishing magnetic field D_μ and t^i commutes with each other,

$$\bar{\psi}\gamma_\mu D_\mu\psi \rightarrow \bar{\psi}(x)\gamma_\mu D_\mu\psi(x) - \alpha^i(x)\partial_\mu(\bar{\psi}(x)\gamma_\mu t^i\gamma_5\psi(x)). \quad (\text{A.13})$$

The variational part from the action is,

$$\frac{\delta S_{\text{QCD}}}{\delta\alpha^i(x)} = -\partial_\mu(\bar{\psi}(x)\gamma_\mu t^i\gamma_5\psi(x)) + 2m\bar{\psi}(x)t^i\gamma_5\psi(x). \quad (\text{A.14})$$

b. Non-zero magnetic field We focus on the traceless part, namely we only take $i = 1, 2, 3$. The kinetic term is transformed as,

$$\bar{\psi}\gamma_\mu\tilde{D}_\mu\psi \rightarrow \bar{\psi}(x)\gamma_\mu\tilde{D}_\mu\psi(x) + \bar{\psi}(x)\gamma_\mu(\partial_\mu\alpha^i(x))t^i\gamma_5\psi(x) - e\alpha^i(x)A_\mu\bar{\psi}(x)\gamma_\mu\gamma_5T_i^{12}\psi(x). \quad (\text{A.15})$$

The variational part from the action is,

$$\frac{\delta S_{\text{QCD}}}{\delta\alpha^i(x)} = -\partial_\mu(\bar{\psi}(x)\gamma_\mu t^i\gamma_5\psi(x)) + 2m\bar{\psi}(x)t^i\gamma_5\psi(x) + \Delta_i(x, eB), \quad (\text{A.16})$$

where

$$\Delta_i(x, eB) = -eA_\mu(x)\bar{\psi}(x)\gamma_\mu\gamma_5T_i^{12}\psi(x). \quad (\text{A.17})$$

For the magnetic field in the Landau gauge, i.e. $A_\mu(x) = (0, Bx_1, 0, 0)$, we have

$$\Delta_i(x, eB) = -eBx_1\bar{\psi}(x)\gamma_2\gamma_5(\delta_{i2}t^1 - \delta_{i1}t^2)\psi(x). \quad (\text{A.18})$$

Since the Dirac fields transform as $\bar{\psi}(t, \vec{x}) \rightarrow \bar{\psi}(t, -\vec{x})\gamma^0$, $\psi(t, \vec{x}) \rightarrow \gamma^0\psi(t, -\vec{x})$ under the parity, and the bilinear term transforms as the odd parity, $x_1\bar{\psi}\gamma_2\gamma_5\psi(t, \vec{x}) \rightarrow -x_1\bar{\psi}\gamma_2\gamma_5\psi(t, -\vec{x})$, $\Delta_i(x, eB)$ is an odd function of x_1 .

2. Chiral rotation for observables

We show the derivation of $\frac{\delta O}{\delta\alpha^i(x)}$ with the chiral rotation for pseudo-scalar and vector operators in this subsection as follows.

a. Chiral rotation for pseudo-scalar operator The pseudo-scalar operator for the SU(2) case is $P^i(y) = \bar{\psi}(y)\gamma_5 t^i\psi(y)$, where $i = 1, 2, 3$. It transforms as,

$$\bar{\psi}(y)\gamma_5 t^i\psi(y) \rightarrow \bar{\psi}(y)\gamma_5 t^i\psi(y) + \frac{1}{2}\alpha^i(y)\bar{\psi}(y)\psi(y). \quad (\text{A.19})$$

Thus the variation is,

$$\frac{\delta P^i(y)}{\delta\alpha^j(x)} = \frac{\delta(\bar{\psi}(y)\gamma_5 t^i\psi(y))}{\delta\alpha^j(x)} = \frac{1}{2}\bar{\psi}(y)\psi(y)\delta(x-y)\delta^{ij}. \quad (\text{A.20})$$

b. Chiral rotation for vector current operator A vector current operator is defined as $V_i^\mu(y) = \bar{\psi}(y)\gamma_\mu t^i\psi(y)$. It transforms under the chiral transformation as,

$$\bar{\psi}(y)\gamma_\mu t^i\psi(y) \rightarrow \bar{\psi}(y)\gamma_\mu t^i\psi(y) - i\alpha^j(y)\epsilon^{ikj}\bar{\psi}(y)t^k\gamma_\mu\gamma_5\psi(y), \quad (\text{A.21})$$

where ϵ^{ikj} is the anti-symmetric tensor. The corresponding variation term is then expressed as,

$$\frac{\delta V_i^\mu(y)}{\delta\alpha^j(x)} = \frac{\delta(\bar{\psi}(y)\gamma_\mu t^i\psi(y))}{\delta\alpha^j(x)} = -i\delta(x-y)\epsilon^{ikj}\bar{\psi}(y)t^k\gamma_\mu\gamma_5\psi(y). \quad (\text{A.22})$$

3. Non-anomalous Ward-Takahashi identity

With the variations derived in Appendices A 1 and A 2, we are ready to derive the Ward-Takahashi identities for the non-anomalous case,

$$\left\langle O \frac{\delta S_{\text{QCD}}}{\delta\alpha^j(x)} \right\rangle = \left\langle \frac{\delta O}{\delta\alpha^j(x)} \right\rangle, \quad (\text{A.23})$$

for chiral rotations with pseudo-scalar and vector operators as follows in the nonzero magnetic field.

a. *Chiral rotation with pseudo-scalar operator*

We choose an operator as $O(y) = P^j(y) = \bar{\psi}(y)\gamma_5 t^j \psi(y)$. The left hand side of Eq. A.23 is,

$$\text{LHS} = -\partial_\mu^x \langle P^j(y) (\bar{\psi}(x)\gamma_\mu t^i \gamma_5 \psi(x)) \rangle + 2m \langle P^j(y) \bar{\psi}(x) t^i \gamma_5 \psi(x) \rangle + \langle P^j(y) \Delta_i(x, eB) \rangle, \quad (\text{A.24})$$

By integrating over x , and the first term vanishes,

$$\int d^4x \text{LHS} = 2m \int d^4x \langle P^j(y) P^i(x) \rangle + \int d^4x \langle P^j(y) \Delta_i(x, eB) \rangle. \quad (\text{A.25})$$

$$(\text{A.26})$$

And the right hand side of Eq. A.23 is,

$$\text{RHS} = \left\langle \frac{\delta P^j(y)}{\delta \alpha^i(x)} \right\rangle = \frac{1}{2} \langle \bar{\psi}(y) \psi(y) \rangle \delta(x-y) \delta^{ij}. \quad (\text{A.27})$$

Integrating over x we arrive at

$$\int d^4x \text{RHS} = \left\langle \frac{\delta P^j(y)}{\delta \alpha^i(x)} \right\rangle = \frac{1}{2} \langle \bar{\psi}(y) \psi(y) \rangle \delta^{ij}. \quad (\text{A.28})$$

Thus the identity becomes,

$$4m \int d^4x \langle P^j(y) P^i(x) \rangle + 2 \int d^4x \langle P^j(y) \Delta_i(x, eB) \rangle = \langle \bar{\psi}(y) \psi(y) \rangle \delta^{ij}. \quad (\text{A.29})$$

Integrating over y and dividing by four-volume V ,

$$4m \frac{1}{V} \int d^4y d^4x \langle P^i(y) P^j(x) \rangle + \frac{2}{V} \int d^4y \int d^4x \langle P^j(y) \Delta_i(x, eB) \rangle = \frac{1}{V} \int d^4y \langle \bar{\psi}(y) \psi(y) \rangle \delta^{ij}. \quad (\text{A.30})$$

In our convention the right hand side of the above identity gives a two-flavor chiral condensate, i.e. $\langle \bar{\psi} \psi \rangle_u + \langle \bar{\psi} \psi \rangle_d$ with $i = j$. At nonzero magnetic field the neutral pion operator is $\alpha(\bar{u}\gamma_5 u - \beta\bar{d}\gamma_5 d)$ with $\alpha^2 + \beta^2 = 1$, thus in the case of $i = j = 3$ and $\alpha = \beta = 1/\sqrt{2}$ the left hand side of the above identity is proportional to the correlation function of neutral pion. Note that when $i = 3$ for the magnetic field related term $\Delta_i(x, eB)$ (cf. Eq. A.18) itself vanishes. The above identity thus becomes

$$2m_l \chi_{\pi^0} = \langle \bar{\psi} \psi \rangle_u + \langle \bar{\psi} \psi \rangle_d. \quad (\text{A.31})$$

The above relation can also be extended to the cases involving the strange quark,

$$m_s \chi_{\eta_s^0} = \langle \bar{\psi} \psi \rangle_s, \quad (\text{A.32})$$

$$(m_d + m_s) \chi_{K^0} = \langle \bar{\psi} \psi \rangle_d + \langle \bar{\psi} \psi \rangle_s. \quad (\text{A.33})$$

Here χ_{π^0} , $\chi_{\eta_s^0}$ and χ_{K^0} are the space-time sum of the two-point correlation functions for neutral pion, $\eta_s^0(s\bar{s})$ and neutral kaon, and $m_l = m_u = m_d$.

The identity A.31 at zero magnetic field was also obtained using a diagrammatic method [63]. Since the magnetic field represented by the $U(1)$ field can be factored out from the gauge field the extension to nonzero magnetic field remains the same, which can be simply observed from the diagrammatic method in [63]. As seen from Fig. 3 and the discussions in Section III C the identities A.31, A.32 and A.33 hold well in the staggered discretization scheme.

b. *Chiral rotation with vector current operator*

The left hand side of Eq. A.23 for the case of the vector current operator is,

$$\text{LHS} = -\langle V_j^\mu(y) \partial_\mu^x (\bar{\psi}(x)\gamma_\mu t^i \gamma_5 \psi(x)) \rangle + 2m \langle V_j^\mu(y) \bar{\psi}(x) t^i \gamma_5 \psi(x) \rangle + \langle V_j^\mu(y) \Delta_i(x, eB) \rangle, \quad (\text{A.34})$$

Integrating over x and using $P^i(x) = \bar{\psi}(x)\gamma_5 t^i \psi(x)$,

$$\int d^4x \text{LHS} = 2m \int d^4x \langle V_j^\mu(y) P^i(x) \rangle + \int d^4x \langle V_j^\mu(y) \Delta_i(x, eB) \rangle, \quad (\text{A.35})$$

The right hand side of Eq. A.23 with integration for x can be expressed as

$$\int d^4x \left\langle \frac{\delta V_j^\mu(y)}{\delta \alpha^i(x)} \right\rangle = -2i \epsilon^{ikj} \langle \bar{\psi}(y) t^k \gamma_\mu \gamma_5 \psi(y) \rangle, \quad (\text{A.36})$$

By combining them and integrating over y we arrive at

$$2m \int d^4x d^4y \langle V_j^\mu(y) P^i(x) \rangle + \int d^4x d^4y \langle V_j^\mu(y) \Delta_i(x, eB) \rangle = -2i \epsilon^{ikj} \int d^4y \langle \bar{\psi}(y) t^k \gamma_\mu \gamma_5 \psi(y) \rangle. \quad (\text{A.37})$$

Appendix B: Simulations in the HISQ discretization scheme

In this appendix we describe the implementation of the magnetic field in the lattice QCD simulations using the HISQ action and in particular the procedure to compute the fermion force. The HISQ action is constructed by the Kogut-Susskind 1-link action D_{KS} and Naik improvement term D_{Naik} with smeared links,

$$D_{\text{HISQ}}[X(U), W(U)] \equiv c_{1000} D_{\text{KS}}[X(U)] + c_{3000} D_{\text{Naik}}[W(U)], \quad (\text{B.1})$$

where all coefficients are chosen at vanishing magnetic field [85] and

$$D_{\text{KS}}[X(U)] = \sum_{\mu} \eta_{\mu}(n) [X_{\mu}(n) \delta_{n+\mu, n'} - X_{\mu}^{\dagger}(n - \hat{\mu}) \delta_{n-\mu, n'}], \quad (\text{B.2})$$

and

$$D_{\text{Naik}}[W(U)] = \sum_{\mu} \eta_{\mu}(n) [W_{\mu}(n) W_{\mu}(n + \hat{\mu}) W_{\mu}(n + 2\hat{\mu}) \delta_{n+3\mu, n'} - W_{\mu}^{\dagger}(n - \hat{\mu}) W_{\mu}^{\dagger}(n - 2\hat{\mu}) W_{\mu}^{\dagger}(n - 3\hat{\mu}) \delta_{n-3\mu, n'}], \quad (\text{B.3})$$

where $\eta_{\mu}(n)$ is the staggered phase, X denotes level-two fat-7 smeared links and W denotes re-unitarized links, which are constructed by thin links U .

The magnetic field on the lattice is represented by U(1) links in the Landau gauge for the electric charge q ,

$$\begin{aligned} u_x(n_x, n_y, n_z, n_t) &= \begin{cases} \exp[-iq\hat{B}N_x n_y], & (n_x = N_x - 1) \\ 1 & (\text{otherwise}) \end{cases} \\ u_y(n_x, n_y, n_z, n_t) &= \exp[iq\hat{B}n_x], \\ u_z(n_x, n_y, n_z, n_t) &= u_t(n_x, n_y, n_z, n_t) = 1, \end{aligned}$$

where $\hat{B} = a^2 B$ with the lattice spacing a . In the HISQ action, the magnetic field can be realized by just replacing all smeared links as

$$D_{\text{HISQ}}[X, W] \rightarrow D_{\text{HISQ}}[uX, uW]. \quad (\text{B.4})$$

while keeping the bare links in the gauge action because gluons do not carry electric charges. Note that we multiply the magnetic field to the smeared links instead of bare links, which could be different from the case in the implementation of imaginary chemical potential as the magnetic field variable u depends on the coordinate. We suppress the Naik term contribution for simplicity below but the extension is straightforward.

We employ the RHMC algorithm to generate gauge configurations. The fermion force is defined as,

$$F_{\mu}(n) = \left[U_{\mu}(n) \frac{\partial S_{\text{f}}[X]}{\partial U_{\mu}(n)} \right]_{\text{TA}} \quad (\text{no sum}), \quad (\text{B.5})$$

where S_{f} is rationally approximated pseudofermion action and TA means removing-trace and anti-hermitianizing operations. In the presence of magnetic fields the force is modified as,

$$F_{\mu}(n) = \left[U_{\mu}(n) \frac{\partial S_{\text{f}}[uX]}{\partial U_{\mu}(n)} \right]_{\text{TA}} \quad (\text{no sum}). \quad (\text{B.6})$$

For the case of zero magnetic field the derivative with respect to bare links can be calculated with the chain rule, which can be symbolically expressed as

$$\frac{\partial S_f[X]}{\partial U} = \frac{\partial S_f[X]}{\partial X} \frac{\partial X}{\partial W} \frac{\partial W}{\partial V} \frac{\partial V}{\partial U}, \quad (\text{B.7})$$

where V is the level one fat-7 link. The first term on the right hand side $\partial S_f[X]/\partial X$ is formally same function form as the standard staggered force except that smeared links are used instead of thin links. This term can be symbolically written as:

$$\frac{\partial S_f[X]}{\partial X} \sim \sum_k \psi_k^\dagger \otimes \Psi_k + \dots \quad (\text{B.8})$$

where $\Psi_k = (D_{\text{HISQ}}^\dagger[X]D_{\text{HISQ}}[X] + \beta_k)^{-1}\phi$, $\psi_k = D_{\text{HISQ}}[X]\Psi_k$ and ϕ is a pseudo-fermion field and β_k represents a rational coefficient of order k . For the case of nonzero magnetic field Eq. B.7 becomes,

$$\frac{\partial S_f[uX]}{\partial U} = \frac{\partial S_f[uX]}{\partial X} \frac{\partial X}{\partial W} \frac{\partial W}{\partial V} \frac{\partial V}{\partial U}. \quad (\text{B.9})$$

Since X, W , and V are dummy variables in the chain rule, the above term can be rewritten as,

$$\frac{\partial S_f[uX]}{\partial U} = \frac{\partial S_f[\tilde{X}]}{\partial \tilde{X}} \frac{\partial \tilde{X}}{\partial W} \frac{\partial W}{\partial V} \frac{\partial V}{\partial U}, \quad (\text{B.10})$$

where variables with tilde represent U(1) rotated variables $\tilde{X} = uX$. Thus the functional form of the first term on the right hand side of the equal sign is the same as that at zero magnetic field (cf. Eq. B.7). Moreover, in the second term, magnetic field is just factored out as $\partial \tilde{X}/\partial W = u\partial X/\partial W$ due to the structure of fat-7 links. Finally in the presence of magnetic fields the fermion force is,

$$F_\mu^{\text{mag-HISQ}}(n) = [u_\mu(n)U_\mu(n)\mathcal{F}]_{\text{TA}} \quad (\text{no sum}) \quad (\text{B.11})$$

with

$$\mathcal{F} = \left. \frac{\partial S_f}{\partial X} \right|_{X \rightarrow uX} \frac{\partial X}{\partial W} \frac{\partial W}{\partial V} \frac{\partial V}{\partial U}, \quad (\text{B.12})$$

where $\left. \frac{\partial S_f}{\partial X} \right|_{X \rightarrow uX}$ means that the staggered force term with an argument uX instead of X . Thus the force calculation in the molecular dynamics is summarized as follows,

1. Prepare smeared links X, W and V from U ,
2. Multiply U(1) variable u on the smeared links X ,
3. Calculate a part of fermion force, $\Psi_k = (D_{\text{HISQ}}^\dagger[uX]D_{\text{HISQ}}[uX] + \beta_k)^{-1}\phi$ and $\psi_k = D_{\text{HISQ}}[X]\Psi_k$ for all k for the rational approximation,
4. Remove U(1) variable u from the smeared links uX ,
5. Construct \mathcal{F} ,
6. Finalize the force $F_\mu^{\text{mag-HISQ}}(n)$.

-
- [1] D. E. Kharzeev, L. D. McLerran, and H. J. Warringa, The Effects of topological charge change in heavy ion collisions: 'Event by event P and CP violation', *Nucl. Phys.* **A803**, 227 (2008), [arXiv:0711.0950 \[hep-ph\]](#).
- [2] V. Skokov, A. Yu. Illarionov, and V. Toneev, Estimate of the magnetic field strength in heavy-ion collisions, *Int. J. Mod. Phys.* **A24**, 5925 (2009), [arXiv:0907.1396 \[nucl-th\]](#).
- [3] W.-T. Deng and X.-G. Huang, Event-by-event generation of electromagnetic fields in heavy-ion collisions, *Phys. Rev.* **C85**, 044907 (2012), [arXiv:1201.5108 \[nucl-th\]](#).
- [4] T. Vachaspati, Magnetic fields from cosmological phase transitions, *Phys. Lett.* **B265**, 258 (1991).

- [5] K. Enqvist and P. Olesen, On primordial magnetic fields of electroweak origin, *Physics Letters B* **319**, 178 (1993).
- [6] M. D’Elia, S. Mukherjee, and F. Sanfilippo, QCD Phase Transition in a Strong Magnetic Background, *Phys. Rev.* **D82**, 051501 (2010), [arXiv:1005.5365 \[hep-lat\]](#).
- [7] I. A. Shovkovy, Magnetic Catalysis: A Review, *Lect. Notes Phys.* **871**, 13 (2013), [arXiv:1207.5081 \[hep-ph\]](#).
- [8] H.-T. Ding, C. Schmidt, A. Tomiya, and X.-D. Wang, Chiral phase structure of three flavor QCD in a background magnetic field, (2020), [arXiv:2006.13422 \[hep-lat\]](#).
- [9] G. S. Bali, F. Bruckmann, G. Endrodi, Z. Fodor, S. D. Katz, S. Krieg, A. Schafer, and K. K. Szabo, The QCD phase diagram for external magnetic fields, *JHEP* **02**, 044, [arXiv:1111.4956 \[hep-lat\]](#).
- [10] G. S. Bali, F. Bruckmann, G. Endrodi, Z. Fodor, S. D. Katz, and A. Schafer, QCD quark condensate in external magnetic fields, *Phys. Rev.* **D86**, 071502 (2012), [arXiv:1206.4205 \[hep-lat\]](#).
- [11] E. M. Ilgenfritz, M. Muller-Preussker, B. Petersson, and A. Schreiber, Magnetic catalysis (and inverse catalysis) at finite temperature in two-color lattice QCD, *Phys. Rev.* **D89**, 054512 (2014), [arXiv:1310.7876 \[hep-lat\]](#).
- [12] V. G. Bornyakov, P. V. Buividovich, N. Cundy, O. A. Kochetkov, and A. Schäfer, Deconfinement transition in two-flavor lattice QCD with dynamical overlap fermions in an external magnetic field, *Phys. Rev.* **D90**, 034501 (2014), [arXiv:1312.5628 \[hep-lat\]](#).
- [13] G. S. Bali, F. Bruckmann, G. Endrodi, S. D. Katz, and A. Schäfer, The QCD equation of state in background magnetic fields, *JHEP* **08**, 177, [arXiv:1406.0269 \[hep-lat\]](#).
- [14] A. Tomiya, H.-T. Ding, X.-D. Wang, Y. Zhang, S. Mukherjee, and C. Schmidt, Phase structure of three flavor QCD in external magnetic fields using HISQ fermions, *Proceedings, 36th International Symposium on Lattice Field Theory (Lattice 2018): East Lansing, MI, United States, July 22-28, 2018*, *PoS LATTICE2018*, 163 (2019), [arXiv:1904.01276 \[hep-lat\]](#).
- [15] M. D’Elia and F. Negro, Chiral Properties of Strong Interactions in a Magnetic Background, *Phys. Rev. D* **83**, 114028 (2011), [arXiv:1103.2080 \[hep-lat\]](#).
- [16] J. O. Andersen, W. R. Naylor, and A. Tranberg, Phase diagram of QCD in a magnetic field: A review, *Rev. Mod. Phys.* **88**, 025001 (2016), [arXiv:1411.7176 \[hep-ph\]](#).
- [17] T. Kojo and N. Su, The quark mass gap in a magnetic field, *Phys. Lett.* **B720**, 192 (2013), [arXiv:1211.7318 \[hep-ph\]](#).
- [18] F. Bruckmann, G. Endrodi, and T. G. Kovacs, Inverse magnetic catalysis and the Polyakov loop, *JHEP* **04**, 112, [arXiv:1303.3972 \[hep-lat\]](#).
- [19] K. Fukushima and Y. Hidaka, Magnetic Catalysis Versus Magnetic Inhibition, *Phys. Rev. Lett.* **110**, 031601 (2013), [arXiv:1209.1319 \[hep-ph\]](#).
- [20] M. Ferreira, P. Costa, O. Lourenço, T. Frederico, and C. Providência, Inverse magnetic catalysis in the (2+1)-flavor Nambu-Jona-Lasinio and Polyakov-Nambu-Jona-Lasinio models, *Phys. Rev.* **D89**, 116011 (2014), [arXiv:1404.5577 \[hep-ph\]](#).
- [21] L. Yu, H. Liu, and M. Huang, Spontaneous generation of local CP violation and inverse magnetic catalysis, *Phys. Rev. D* **90**, 074009 (2014), [arXiv:1404.6969 \[hep-ph\]](#).
- [22] B. Feng, D. Hou, H.-c. Ren, and P.-p. Wu, Bose-Einstein Condensation of Bound Pairs of Relativistic Fermions in a Magnetic Field, *Phys. Rev. D* **93**, 085019 (2016), [arXiv:1512.08894 \[hep-ph\]](#).
- [23] X. Li, W.-J. Fu, and Y.-X. Liu, Thermodynamics of 2+1 Flavor Polyakov-Loop Quark-Meson Model under External Magnetic Field, *Phys. Rev.* **D99**, 074029 (2019), [arXiv:1902.03866 \[hep-ph\]](#).
- [24] S. Mao, From inverse to delayed magnetic catalysis in a strong magnetic field, *Phys. Rev.* **D94**, 036007 (2016), [arXiv:1605.04526 \[hep-th\]](#).
- [25] U. Gürsoy, I. Iatrakis, M. Järvinen, and G. Nijs, Inverse Magnetic Catalysis from improved Holographic QCD in the Veneziano limit, *JHEP* **03**, 053, [arXiv:1611.06339 \[hep-th\]](#).
- [26] K. Xu, J. Chao, and M. Huang, Spin polarization inducing diamagnetism, inverse magnetic catalysis and saturation behavior of charged pion spectra, (2020), [arXiv:2007.13122 \[hep-ph\]](#).
- [27] M. D’Elia, F. Manigrasso, F. Negro, and F. Sanfilippo, QCD phase diagram in a magnetic background for different values of the pion mass, *Phys. Rev.* **D98**, 054509 (2018), [arXiv:1808.07008 \[hep-lat\]](#).
- [28] G. Endrodi, M. Giordano, S. D. Katz, T. G. Kovács, and F. Pittler, Magnetic catalysis and inverse catalysis for heavy pions, *JHEP* **07**, 007, [arXiv:1904.10296 \[hep-lat\]](#).
- [29] C. Bonati, M. D’Elia, M. Mariti, M. Mesiti, F. Negro, A. Rucci, and F. Sanfilippo, Magnetic field effects on the static quark potential at zero and finite temperature, *Phys. Rev.* **D94**, 094007 (2016), [arXiv:1607.08160 \[hep-lat\]](#).
- [30] M. Gell-Mann, R. J. Oakes, and B. Renner, Behavior of current divergences under $SU(3) \times SU(3)$, *Phys. Rev.* **175**, 2195 (1968).
- [31] P. Boucaud *et al.* (ETM), Dynamical twisted mass fermions with light quarks, *Phys. Lett.* **B650**, 304 (2007), [arXiv:hep-lat/0701012 \[hep-lat\]](#).
- [32] J. Gasser and H. Leutwyler, Chiral Perturbation Theory: Expansions in the Mass of the Strange Quark, *Nucl. Phys. B* **250**, 465 (1985).
- [33] M. Jamin, Flavor symmetry breaking of the quark condensate and chiral corrections to the Gell-Mann-Oakes-Renner relation, *Phys. Lett. B* **538**, 71 (2002), [arXiv:hep-ph/0201174](#).
- [34] J. Bordes, C. Dominguez, P. Moodley, J. Penarrocha, and K. Schilcher, Chiral corrections to the $SU(2) \times SU(2)$ Gell-Mann-Oakes-Renner relation, *JHEP* **05**, 064, [arXiv:1003.3358 \[hep-ph\]](#).
- [35] J. Bordes, C. Dominguez, P. Moodley, J. Penarrocha, and K. Schilcher, Corrections to the $SU(3) \times SU(3)$ Gell-Mann-Oakes-Renner relation and chiral couplings L_8^r and H_2^r , *JHEP* **10**, 102, [arXiv:1208.1159 \[hep-ph\]](#).
- [36] J. Gasser and H. Leutwyler, Light Quarks at Low Temperatures, *Phys. Lett.* **B184**, 83 (1987).
- [37] I. A. Shushpanov and A. V. Smilga, Quark condensate in a magnetic field, *Phys. Lett.* **B402**, 351 (1997), [arXiv:hep-ph/9703201 \[hep-ph\]](#).

- [38] N. O. Agasian and I. A. Shushpanov, Gell-Mann-Oakes-Renner relation in a magnetic field at finite temperature, *JHEP* **10**, 006, [arXiv:hep-ph/0107128](#) [hep-ph].
- [39] H. T. Ding *et al.*, Chiral Phase Transition Temperature in (2+1)-Flavor QCD, *Phys. Rev. Lett.* **123**, 062002 (2019), [arXiv:1903.04801](#) [hep-lat].
- [40] H.-T. Ding, New developments in lattice QCD on equilibrium physics and phase diagram, in *28th International Conference on Ultrarelativistic Nucleus-Nucleus Collisions* (2020) [arXiv:2002.11957](#) [hep-lat].
- [41] K. Hattori, T. Kojo, and N. Su, Mesons in strong magnetic fields: (I) General analyses, *Nucl. Phys.* **A951**, 1 (2016), [arXiv:1512.07361](#) [hep-ph].
- [42] Z. Wang and P. Zhuang, Meson properties in magnetized quark matter, *Phys. Rev.* **D97**, 034026 (2018), [arXiv:1712.00554](#) [hep-ph].
- [43] S. Mao, Pions in magnetic field at finite temperature, *Phys. Rev.* **D99**, 056005 (2019), [arXiv:1808.10242](#) [nucl-th].
- [44] M. Coppola, D. Gomez Dumm, S. Noguera, and N. N. Scoccola, Neutral and charged pion properties under strong magnetic fields in the NJL model, *Phys. Rev.* **D100**, 054014 (2019), [arXiv:1907.05840](#) [hep-ph].
- [45] S. S. Avancini, R. L. S. Farias, and W. R. Tavares, Neutral meson properties in hot and magnetized quark matter: a new magnetic field independent regularization scheme applied to NJL-type model, *Phys. Rev.* **D99**, 056009 (2019), [arXiv:1812.00945](#) [hep-ph].
- [46] K. Xu, S. Shi, H. Zhang, D. Hou, J. Liao, and M. Huang, Extracting the magnitude of magnetic field at freeze-out in heavy-ion collisions, (2020), [arXiv:2004.05362](#) [hep-ph].
- [47] J. Chao, Y.-X. Liu, and L. Chang, Light charged pion in ultra-strong magnetic field, (2020), [arXiv:2007.14258](#) [hep-ph].
- [48] Y. Hidaka and A. Yamamoto, Charged vector mesons in a strong magnetic field, *Phys. Rev.* **D87**, 094502 (2013), [arXiv:1209.0007](#) [hep-ph].
- [49] M. N. Chernodub, Superconductivity of QCD vacuum in strong magnetic field, *Phys. Rev.* **D82**, 085011 (2010), [arXiv:1008.1055](#) [hep-ph].
- [50] M. N. Chernodub, Spontaneous electromagnetic superconductivity of vacuum in strong magnetic field: evidence from the Nambu–Jona-Lasinio model, *Phys. Rev. Lett.* **106**, 142003 (2011), [arXiv:1101.0117](#) [hep-ph].
- [51] E. V. Luschevskaya and O. V. Larina, The ρ and A mesons in a strong abelian magnetic field in $SU(2)$ lattice gauge theory, *Nucl. Phys.* **B884**, 1 (2014), [arXiv:1203.5699](#) [hep-lat].
- [52] G. S. Bali, B. B. Brandt, G. Endrődi, and B. Gläbke, Meson masses in electromagnetic fields with Wilson fermions, *Phys. Rev.* **D97**, 034505 (2018), [arXiv:1707.05600](#) [hep-lat].
- [53] E. V. Luschevskaya, O. E. Solovjeva, O. A. Kochetkov, and O. V. Teryaev, Magnetic polarizabilities of light mesons in $SU(3)$ lattice gauge theory, *Nucl. Phys.* **B898**, 627 (2015), [arXiv:1411.4284](#) [hep-lat].
- [54] E. Luschevskaya, O. Solovjeva, and O. Teryaev, Magnetic polarizability of pion, *Phys. Lett. B* **761**, 393 (2016), [arXiv:1511.09316](#) [hep-lat].
- [55] V. D. Orlovsky and Yu. A. Simonov, Nambu-Goldstone mesons in strong magnetic field, *JHEP* **09**, 136, [arXiv:1306.2232](#) [hep-ph].
- [56] S. Fayazbakhsh and N. Sadooghi, Weak decay constant of neutral pions in a hot and magnetized quark matter, *Phys. Rev.* **D88**, 065030 (2013), [arXiv:1306.2098](#) [hep-ph].
- [57] G. S. Bali, B. B. Brandt, G. Endrődi, and B. Gläbke, Weak decay of magnetized pions, *Phys. Rev. Lett.* **121**, 072001 (2018), [arXiv:1805.10971](#) [hep-lat].
- [58] M. Coppola, D. Gomez Dumm, S. Noguera, and N. N. Scoccola, Pion-to-vacuum vector and axial vector amplitudes and weak decays of pions in a magnetic field, *Phys. Rev.* **D99**, 054031 (2019), [arXiv:1810.08110](#) [hep-ph].
- [59] M. Coppola, D. Gomez Dumm, S. Noguera, and N. N. Scoccola, Magnetic field driven enhancement of the weak decay width of charged pions, (2019), [arXiv:1908.10765](#) [hep-ph].
- [60] M. A. Andreichikov and Yu. A. Simonov, Chiral physics in the magnetic field with quark confinement contribution, *Eur. Phys. J.* **C78**, 902 (2018), [arXiv:1805.11896](#) [hep-ph].
- [61] H.-T. Ding, S.-T. Li, S. Mukherjee, A. Tomiya, and X.-D. Wang, Meson masses in external magnetic fields with HISQ fermions, in *37th International Symposium on Lattice Field Theory (Lattice 2019) Wuhan, Hubei, China, June 16-22, 2019* (2020) [arXiv:2001.05322](#) [hep-lat].
- [62] A. Bazavov, S. Dentinger, H.-T. Ding, *et al.*, Meson screening masses in (2+1)-flavor QCD, *Phys. Rev.* **D100**, 094510 (2019), [arXiv:1908.09552](#) [hep-lat].
- [63] G. W. Kilcup and S. R. Sharpe, A Tool Kit for Staggered Fermions, *Nucl. Phys.* **B283**, 493 (1987).
- [64] S. Aoki *et al.* (JLQCD), Pion decay constant for the Kogut-Susskind quark action in quenched lattice QCD, *Phys. Rev.* **D62**, 094501 (2000), [arXiv:hep-lat/9912007](#) [hep-lat].
- [65] E. Follana, Q. Mason, C. Davies, K. Hornbostel, G. P. Lepage, J. Shigemitsu, H. Trotter, and K. Wong (HPQCD, UKQCD), Highly improved staggered quarks on the lattice, with applications to charm physics, *Phys. Rev.* **D75**, 054502 (2007), [arXiv:hep-lat/0610092](#) [hep-lat].
- [66] H.-T. Ding, F. Karsch, and S. Mukherjee, Thermodynamics of strong-interaction matter from Lattice QCD, *Int. J. Mod. Phys.* **E24**, 1530007 (2015), [arXiv:1504.05274](#) [hep-lat].
- [67] M. Al-Hashimi and U.-J. Wiese, Discrete Accidental Symmetry for a Particle in a Constant Magnetic Field on a Torus, *Annals Phys.* **324**, 343 (2009), [arXiv:0807.0630](#) [quant-ph].
- [68] A. Bazavov, T. Bhattacharya, M. Cheng, C. DeTar, H.-T. Ding, *et al.*, The chiral and deconfinement aspects of the QCD transition, *Phys. Rev.* **D85**, 054503 (2012), [arXiv:1111.1710](#) [hep-lat].
- [69] H. Akaike, A new look at the statistical model identification, *IEEE Transactions on Automatic Control* **19**, 716 (1974).
- [70] J. E. Cavanaugh, Unifying the derivations for the akaike and corrected akaike information criteria, *Statistics & Probability*

Letters **33**, 201 (1997).

- [71] C. W. Bernard, M. C. Ogilvie, T. A. DeGrand, C. E. DeTar, S. A. Gottlieb, A. Krasnitz, R. L. Sugar, and D. Toussaint, The Spatial structure of screening propagators in hot QCD, *Phys. Rev. Lett.* **68**, 2125 (1992).
- [72] C. W. Bernard, T. Blum, T. A. DeGrand, C. E. Detar, S. A. Gottlieb, A. Krasnitz, R. L. Sugar, and D. Toussaint, Finite size and quark mass effects on the QCD spectrum with two flavors, *Phys. Rev.* **D48**, 4419 (1993), [arXiv:hep-lat/9305023 \[hep-lat\]](#).
- [73] C. W. Bernard, T. Burch, K. Orginos, D. Toussaint, T. A. DeGrand, C. E. Detar, S. Datta, S. A. Gottlieb, U. M. Heller, and R. Sugar, The QCD spectrum with three quark flavors, *Phys. Rev.* **D64**, 054506 (2001), [arXiv:hep-lat/0104002 \[hep-lat\]](#).
- [74] H.-T. Ding, O. Kaczmarek, F. Karsch, S.-T. Li, S. Mukherjee, A. Tomiya, and Y. Zhang, Dirac Eigenvalue spectrum of $N_f=2+1$ QCD towards the chiral limit using HISQ fermions, in *37th International Symposium on Lattice Field Theory (Lattice 2019) Wuhan, Hubei, China, June 16-22, 2019* (2019) [arXiv:2001.05217 \[hep-lat\]](#).
- [75] L. Giusti and M. Luscher, Chiral symmetry breaking and the Banks-Casher relation in lattice QCD with Wilson quarks, *JHEP* **03**, 013, [arXiv:0812.3638 \[hep-lat\]](#).
- [76] G. Cossu, H. Fukaya, S. Hashimoto, T. Kaneko, and J.-I. Noaki, Stochastic calculation of the Dirac spectrum on the lattice and a determination of chiral condensate in 2+1-flavor QCD, *PTEP* **2016**, 093B06 (2016), [arXiv:1607.01099 \[hep-lat\]](#).
- [77] Z. Fodor, K. Holland, J. Kuti, S. Mondal, D. Negradi, and C. H. Wong, New approach to the Dirac spectral density in lattice gauge theory applications, *Proceedings, 33rd International Symposium on Lattice Field Theory (Lattice 2015): Kobe, Japan, July 14-18, 2015*, *PoS LATTICE2015*, 310 (2016), [arXiv:1605.08091 \[hep-lat\]](#).
- [78] F. X. Lee, L. Zhou, W. Wilcox, and J. C. Christensen, Magnetic polarizability of hadrons from lattice QCD in the background field method, *Phys. Rev. D* **73**, 034503 (2006), [arXiv:hep-lat/0509065](#).
- [79] C. Adolph *et al.* (COMPASS), Measurement of the charged-pion polarizability, *Phys. Rev. Lett.* **114**, 062002 (2015), [arXiv:1405.6377 \[hep-ex\]](#).
- [80] T. D. Cohen, D. A. McGady, and E. S. Werbos, The Chiral condensate in a constant electromagnetic field, *Phys. Rev.* **C76**, 055201 (2007), [arXiv:0706.3208 \[hep-ph\]](#).
- [81] E. S. Werbos, The Chiral condensate in a constant electromagnetic field at $O(p^*6)$, *Phys. Rev.* **C77**, 065202 (2008), [arXiv:0711.2635 \[hep-ph\]](#).
- [82] S. Aoki *et al.* (Flavour Lattice Averaging Group), FLAG Review 2019: Flavour Lattice Averaging Group (FLAG), *Eur. Phys. J. C* **80**, 113 (2020), [arXiv:1902.08191 \[hep-lat\]](#).
- [83] J. C. Ward, An Identity in Quantum Electrodynamics, *Phys. Rev.* **78**, 182 (1950).
- [84] Y. Takahashi, On the generalized Ward identity, *Nuovo Cim.* **6**, 371 (1957).
- [85] A. Bazavov *et al.* (MILC), Scaling studies of QCD with the dynamical HISQ action, *Phys. Rev.* **D82**, 074501 (2010), [arXiv:1004.0342 \[hep-lat\]](#).